The Gottfried Wilhelm Leibniz University Hannover
Hannover Centre for Optical Technologies

Master Thesis

Tip Convolution Effects and their Deconvolution in Photo-Indcued Force Microscopy

Author
Hardikkumar Gadher
(10018238)

Supervisor
Prof. Dr. Bernhard Roth

Examiner
Dr. Daniela Täuber

November 2021

Department of Microscopy
Leibniz Institute of Photonic Technology, Jena

Declaration

I hereby declare that the thesis work submitted is the result of entirely independent research carried out solely under the supervision of my supervisor. Except for the acknowledged publications, the document does not contain the research results that others have written or published, to the best of my knowledge. Individuals and organizations who made significant contributions to this paper's research have been acknowledged in the text. This thesis work has also never been submitted for any other qualification or professional certification.

Jena, 11.11.2021

Hardikkumar Gadher

Acknowledgement

As I close the end of my master's degree, I would like to take this opportunity to thank everyone who helped me with my master's thesis and guided me through a difficult situation.

I want to express my gratitude and appreciation to all those who gave me the possibility to complete this master thesis. I want to thank Prof. Dr Bernhard Roth, who supervised me throughout my thesis work.

I want to thank Dr Daniela Täuber, who offered to work with the Microscopy team under the Leibniz Institute of Photonic Technology. I would not miss the chance to express my gratitude to her for believing in me throughout this work. I appreciate her efforts in guiding students like me and empowering their scientific skills.

Significant thanks to Leibniz-IPHT, Jena, who allowed me to work with the Microscopy team, especially with the BioPOLIM team.

Abstract

Atomic force microscopy is an advanced method of microscopy to study the engineering of surface roughness. Over the years, a scanning electron microscope has been used to examine the micro-level of samples and structures. Additionally, atomic force microscopy has played a vital role in every aspect of microbiology or biophotonics. Studying a surface gives complete detailed numerical data of the surface and its characterization. This thesis covers a study of atomic force microscopy and its comprehensive technologies. Photo-induced force microscopy is an advancement of atomic force microscopy. In this study of Photo-induced force microscopy, various parameters like tip information, surface convolution, sample deconvolution and their methods have been carried out. This study mainly focuses on the convolution artefacts of the imaging process and idea generation of how this error could be compensated. Several developments occurred in microscopy either to get rid of human errors or machine errors. These optimized developments regarding the various context of imaging samples are described in this thesis and studied to develop a convincing conclusion.

Table of Contents

List of Figures

List of Abbreviations

Abbreviations	Description
AFM	Atomic Force Microscopy
FTIR	Fourier-Transform Infrared Spectroscopy
SNOM	Scanning Near-field Optical microscopy
STM	Scanning Tunneling Microscopy
PiFM	Photo-Induced Force Microscopy
TEM	Transmission Electron Microscopy
OM	Optical Microscopy
SEM	Scanning Electron Microscopy
vdW	van der Waals Force

List of Tables

1. Introduction

The suggested photo-induced force microscopy is an extended method of atomic force microscopy. Atomic force microscopy is an emerging method to extract the data of microstructure and nanomaterials. The form of objective remains equal in photo-induced force microscopy as atomic force microscopy. Still, the other force coerced to illuminate the molecules from the surface to the tip is advanced. Further emphasizing, this can be infrared or other optical light sources, which need to be installed. [2][3]

To overcome the problems and limits of s-SNOM/nano-FTIR, Wickramasinghe introduced photo-induced force microscopy (PiFM). This ground-breaking technology measures the near-field optical interaction between the tip and sample using mechanical rather than optical detection. PiFM was first developed for optical illumination of the tip-sample region, resulting in highly localized forces that AFM quickly measures between the tip and sample.[4][2]

Various kinds of nanomaterials are considered to get tested in PiFM. The AFM probe is being brought to the proximity of the sample in an approach operation, and new contours would come across in the raster scan. Different AFM probe types need to be mounted according to the user's familiarity with the sample surface. Each test avails a foreign surface structure to get familiar with because there is a formalism of artefacts. These artefacts convolute the topography and do not give the contours scanned images as exactly in original images. Artefacts might differ by all kind of geometry forms. Thus, familiarity with surface and tip would perform a vital role while going through AFM operations. Image artefacts would arise due to various factors in routine. Those must be omitted or decreased to have the utmost topography as the original image, and they are defined as deconvolution methods and as a result of this further studied.

Various convolution effects due to a variety of circumstances have been investigated and reviewed in this thesis. Convolution effects do not require any particular output or input; somewhat, they modify the surface roughness according to its natural tendency. Numerous methodologies and conceptions about various AFM parameters have been examined. An overview of the deconvolution methods has been carried out in this work. This overview aims to apply photo-induced force microscopy further to understand the impact of the sample topography on the PiFM signal in rough samples. To assess the impact of tip artefacts on the PiFM signal, it is necessary to examine the topography images for evidence of them.

2. Present State of Knowledge

Operations of atomic force microscopy have been studied and prepared the full-scale idea of their process methods. Advancement of any other conventional microscopy has been carried out to probe microscopy.

2.1 Atomic Force Microscopy

Atomic force microscopy is also one of the broad-ranged used microscopies. Unlike other microscopy methods, AFM does not rely on electromagnetic radiation like a photon or electron beams to imaging samples but probes the mechanical interaction with a tiny tip providing nanoscale spatial resolution. AFM is an imaging instrument that is mechanically and optically calibrated to get the sample's topography images and contour properties.[27]

2.2 Intramolecular Forces

The imaging process of the sample roughness carries out in the atomic force microscope to modulate the interaction forces between two atmos. Scientifically, many kinds of forces act from the tip to the surface or the other way around. Still, at this moment of experimenting with force microscopy, intramolecular force is considered. That is significantly driven between the tip surface and the sample surface.[27]

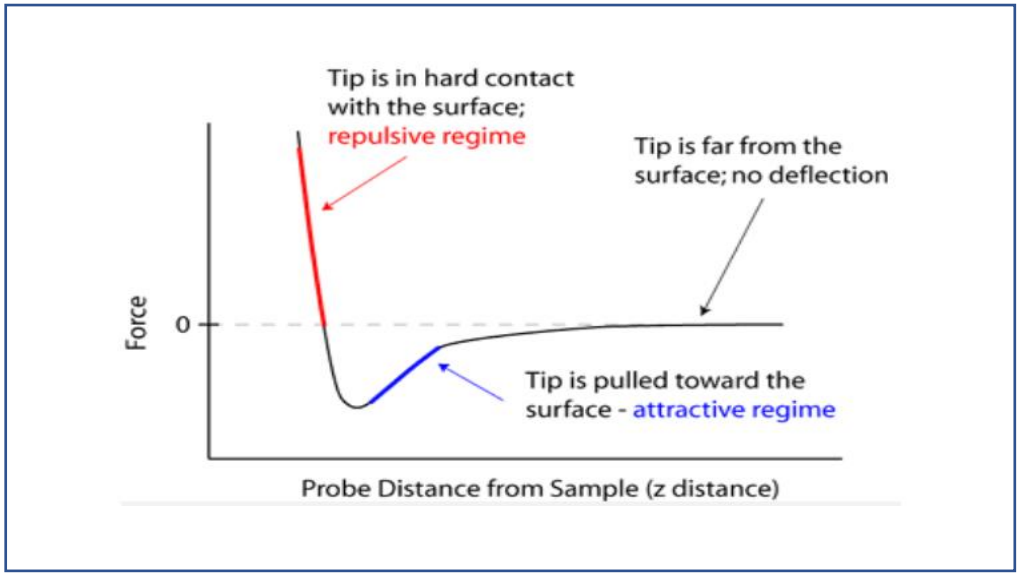

Figure 1 Potential curve of different regimes [7]

AFM works on the surface sensing principle, as a highly sharp tip is used to scan the surface. The tip is the only part that goes to the sample's proximity and measures the texture on the surface. Other features are calibrated to each other and result in the topographical images. As shown in Figure 1, the force coerced between tip and surface depends on the tip-sample separation. As a result of this suggested a brief idea of the Potential curve of these two parameters.[27]

Intermolecular forces between two surfaces or particles according to the nature of the potential curve, with the relation to force and separation distance. As shown in a potential curve, force is acting between two regimes, like repulsive and attractive. When tip and surface are infinitely far away from each other, no interaction occurs between them. As soon as the tip is being brought near to surface to scan, the interaction starts acting. At some point in the curve in the attractive regime, it starts working (approach situation). With this, the separation distance has to be less than or equal to 10nm. This point is the so-called point of contact, where tip and surface come in contact physically.

2.3 Major Components of AFM

As earlier discussed, a Photo-induced force microscope contains AFM itself with some more extending features. To study concepts of PiFM, AFM needs to be gone through by any user wanting PiFM to get run. AFM has four major parts and some extra helping parts to make it a compatible system.

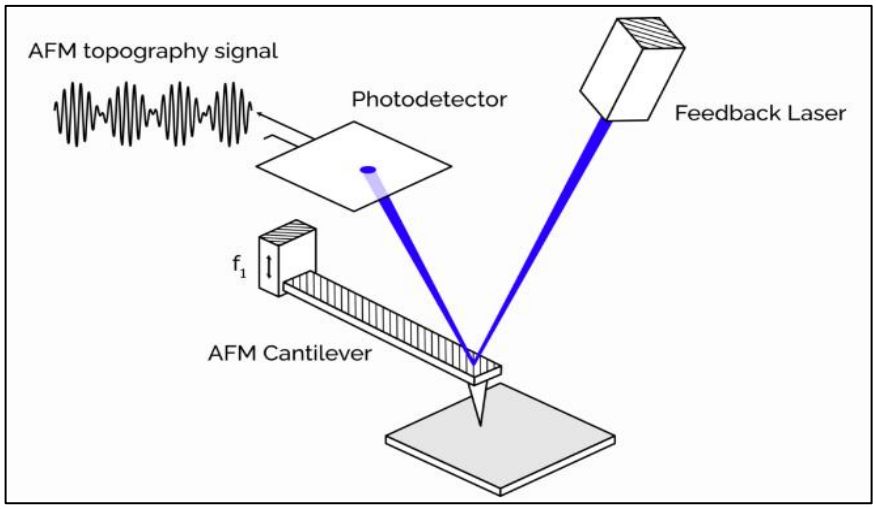

Figure 2 Components of AFM [15]

As mentioned earlier, AFM is mechanically and optically calibrated with different components, where they are equally synchronized and result in imaging of the surface roughness of the sample. Laser beam incidents on the probe cantilever reflected area and reflected onto the photodiode. The photodiode, piezo tube, and feedback control loop are calibrated in real-time to respond to the surface. Piezo tube responds as per its feedback from the photodiode and moves to the occurrence of the intramolecular forces. Each of the AFM components is described as follows:

2.4 AFM Probes or Tips

Tips are an essential component of atomic force microscopy as AFM scans the surface by contacting the surface in contact mode or without contacting the surface in non-contact mode. A tip is the only component that comes to the proximity to the surface

and senses the topography. Commonly tip diameters are 12 to 25 nm. Major study and upcoming scope of AFM optimization rely on the tip geometry and its capability to raster various contours on the surfaces. Mechanically the tip is adhered to the cantilever and runs the raster through the sample. It determines the force applied to the sample and the ultimate resolution of the sample. [3]

Typical examples of AFM probes are tetrahedral, rectangular, pyramidal, and triangular. A good or efficient cantilever can be considered when the cantilever has a low spring constant and higher resonance frequency. AFM head is shown in Figure 3, where the tip and cantilever are mechanically fixed.

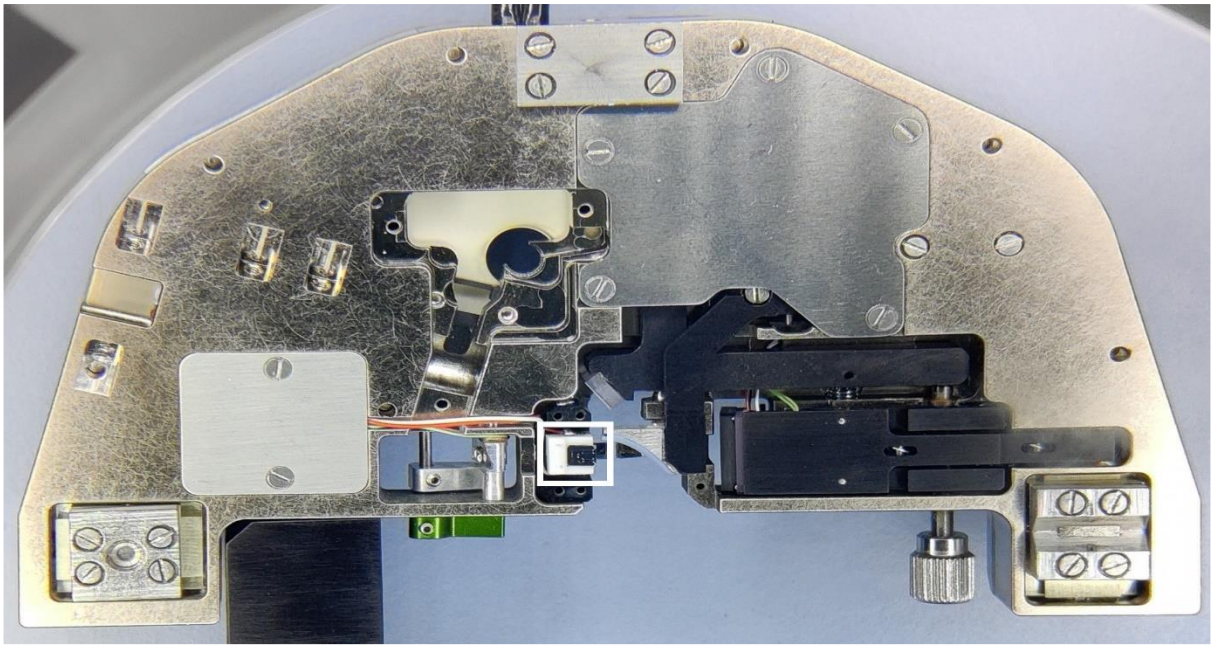

Figure 3 AFM Head showing AFM Tip (Image by courtesy of Dr Täuber)

2.5 Photo Diode (Position sensitive Diode) & Piezo Scanner

The photodiode is used to get light spot falls at the centre or on the periphery. In Quadrant photodiode, any other location than the centre generates finite voltage, and this location has its x-y coordinates to send to the feedback control loop. Piezo scanner elongates and deforms according to its requirement. The sample surface is typically placed on the piezo scanner and moved to get into the attractive regime. [3]

2.6 Operational Aspects

2.6.1 Alignment

Atomic force microscope operates from its tip to the surface and acquires topographical images from the software in the computer. AFM process always starts from the aligning of the tip. AFM setup has two side screws to align the cantilever, and it has to be moved in such a fashion that it comes into the upper contact of the laser

source. The reflecting zone on the top of the cantilever should be at the exact location to get a laser source and reflect it towards QPD. Photodiode also needs to get aligned with screws to focus the laser source to its centre area. The explanation suggested here would be done in the dynamic mode or contact mode of AFM.

2.6.2 Approach

In the attractive regime, the approach is being processed after the alignment of the tip. The potential curve must be studied before getting the concept of approach phenomena of the tip to the surface. As soon as the cantilever comes in the attractive regime or other way round tip is in proximity to the sample surface, the interaction between molecules starts acting. At some point in the potential curve, the cantilever starts deforming before reaching the point of contact, and the force gets activated. A stiff cantilever mostly destructs such forces and does not tend to deform. A more rigid cantilever with a higher spring constant would eliminate this interaction and not bend, unlike any typical cantilever.

2.6.3 Deformation of the tip

At large distances, attractive Van der Waals forces exist, but at close distances, repulsive forces exist due to the overlap of the tip's and sample's electron orbitals. A Lennard-Jones potential can be used to approximate these forces (Figure 6).

There is a threshold separation distance r (Figure 6), so there is an occurance of force interaction that occurs more frequently than the threshold distance. In scenario 1 (Figure 4), It is still less distance to make forces interact. Scenario 2 (Figure 4) is closer to thresold but still not capable of going in the attraction regime, as per given in (Figure 6), Alike these two previous cases, scenario 3 (Figure 4) makes a significant difference and equalizes the threshold distance and moves more downwards to the surface. In this case, the attractive nature of the tip cantilever can be found. One step further in case four cantilever goes more down (having low stiffness), and as the stepper motor is still ON, the cantilever bends. The Figure 5 in contact shows repulsion.

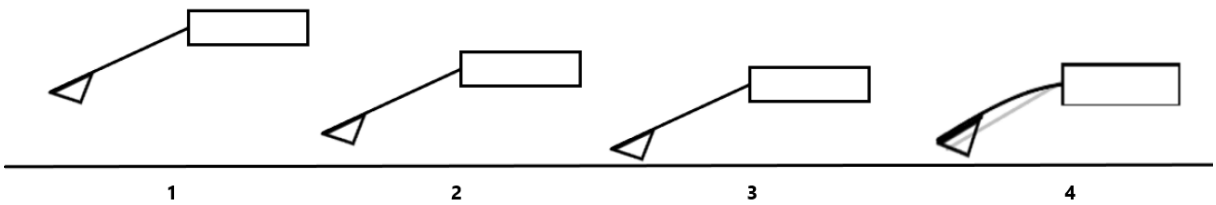

Figure 4 AFM Tip Deformation

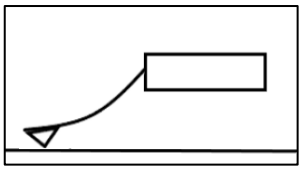

Figure 5 Cantilever is bent in repulsive regime

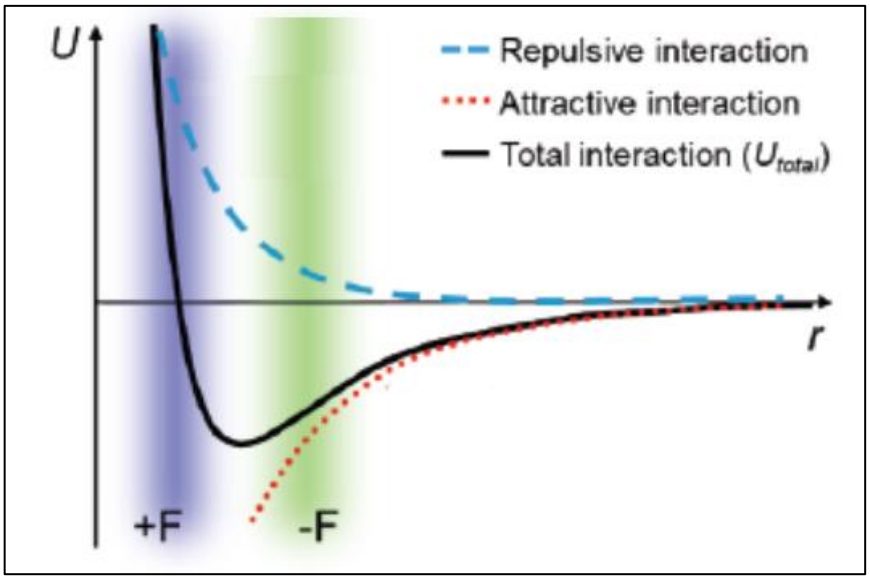

Figure 6 Forces between tip and sample respective of separation distance[28]

Alike in the attractive regime, the cantilever could also move towards a repulsive regime. In Figure 6, this can be found that the repulsive regime profile does not tilt downwards and moves upwards instead. In this case, repulsive forces are found, and the cantilever would bend in another way round of case 4. This can be found in Figure 5 [28].

3. Photo Induced Force Microscopy

This chapter contains AFM functionality and a short introductory study on PiFM functionality and approaches for understanding the physics probed by the gradient force.

A photo-induced force microscopy measures changes in the dipolar contacts between a sharp metallic tip and the material caused by light. [25] Unlike infrared-AFM, photo-induced force microscopy does not rely on the material's thermal expansion. Rather than that, the method is directly sensitive to the electromagnetic forces at work at the tip-sample junction and may be used in non-contact mode AFM in principle.

3.1 Force Microscopy Functionality

Advancing the AFM enhance the capabilities of viewing molecular structures to a nanoscale extent in PiFM.

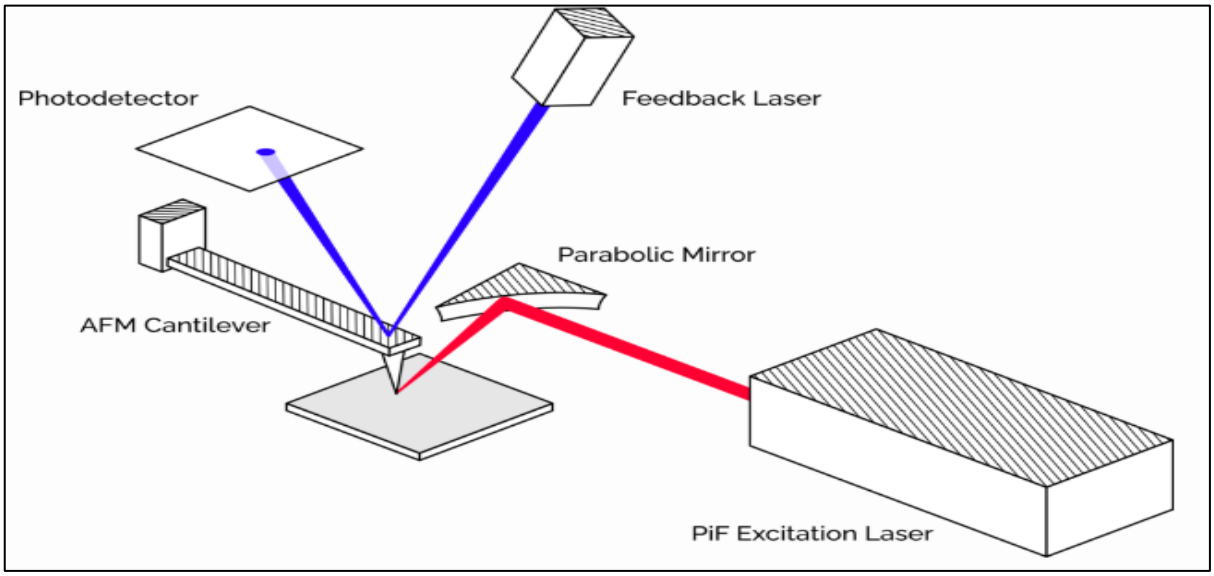

Figure 7 Principle of Photo Induced Force Microscopy [4]

Because PiFM is a relatively new method, few scientists are familiar with it. In brief, PiFM offers chemical imaging (in mid-IR PiFM) in addition to topographical imaging. This is accomplished via the measurement of near optical fields in nanoscale structures using PiFM. PiFM generates spectroscopic data with a spatial resolution of less than 10 nm and a broad-spectrum sensitivity.

3.1.1 Working Principle

As earlier discussed, PiFM itself contains AFM. More features of PiFM are described here with regards to illumination. The working principle of PiFM is mainly focusing on detecting photo-induced force. The tip is used as a conductive one. When it comes to the proximity of the sample while IR radiation is incident arises an attractive force between the induced dipoles in the sample and the tip.

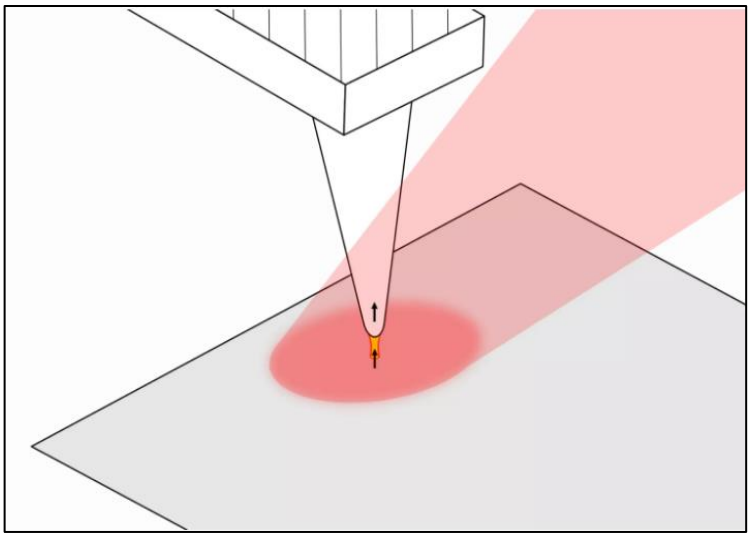

Figure 8 PiFM Sample Surface Illumination using Tunable Lase [15]

At its most fundamental level, an AFM is nothing more than a mechanical resonator in feedback. Mechanical resonators like cantilevers or quartz tuning forks are often utilized in AFMs. A sharp tip is attached to the resonator, making AFM sensitive to topography changes. When the tip is brought into close contact with a surface, it interacts with it, changing the resonator's mechanical characteristics. The topography may be traced by detecting these changes while the tip or sample is scanned relative to one another. Mechanical resonances can be thought of as sensors in this simplistic sense.

3.1.2 Method of Detection

PiFM creates two types of short-range forces at the tip-sample interface: (1) the conventional van der Waals (vdW) force used by non-contact mode AFM to map the topography of the sample surface, and (2) the photo-induced force (PiF) created by near field illumination. Both forces operate on a microscopic scale, becoming active only when the tip is atomically near the sample surface (less than 10 nm). The measured photo-induced force in mid IR mainly is related to the modulation of attractive Van der Waals forces by thermal expansion. Although PiF does not directly measure the VdW-forces, it measures the change of the attractive vdW forces due to thermal expansion. The Z scanner will adjust the amplitude reduction by separating the tip and

sample, allowing the user-specified fixed amplitude to be maintained (the set-point).[6][15]

Side band mode uses frequency mixing. In direct mode, the light frequency does not mix into the detection, as the cantilever is driven at the same frequency which is used for detection via a lock-in amplifier. Due to the cantilever's ability to oscillate even in the absence of a sample, this technique is sensitive to undesired background signal interference. Photo-thermal (bi-metallic and thermal gradient) forces are too responsible for this unwanted excitation, which has nothing to do with the contact between the tip and sample. However, the PiFM direct technique is beneficial because it detects optical interactions deep inside the sample by expanding the sample in response to incoming light that reaches into the sample far below the tip-enhanced illumination zone.

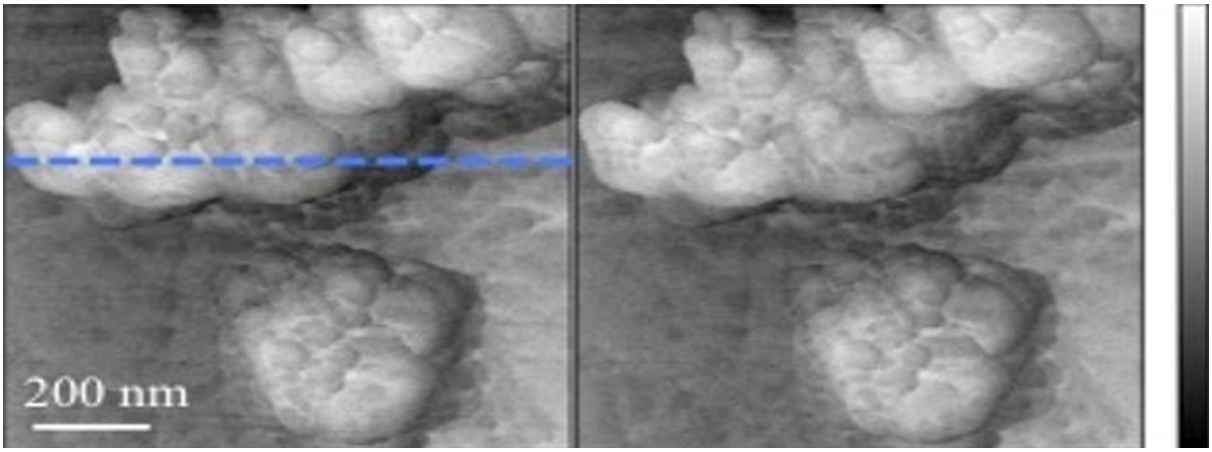

Figure 9 AFM Topography of nano particles [29]

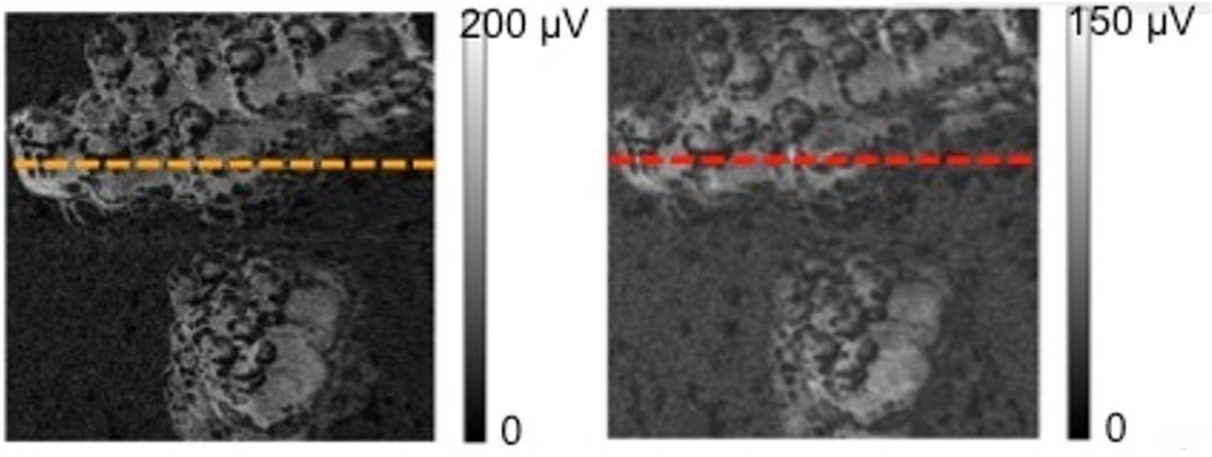

Figure 10 Left: PiFM signal at 880 cm^{-1} of nano particles sample, Right : PiFM signal at 1360 cm^{-1} of nano particles sample [29]

The second modulation technique, sideband detection, eliminates undesirable background signals and restricts the response to a very narrow area at the interface between the tip and the sample. The sideband technique uses frequency mixing to create a difference frequency (sideband) at the cantilever resonance rather than at a resonant cantilever frequency. The laser modulation frequency is selected such that $f_1 = f_o + f_m$, where f_0 and f_1 are the cantilever's first and second mechanical resonances, respectively.[8][11]. Here are some examples for topography (Figure 9) and PiFM signal (Figure 10) of nano particles given for different wavenumbers. The deconvolution in topography images would rises more chances of deconvolution of PiFM signal outputs. [29]

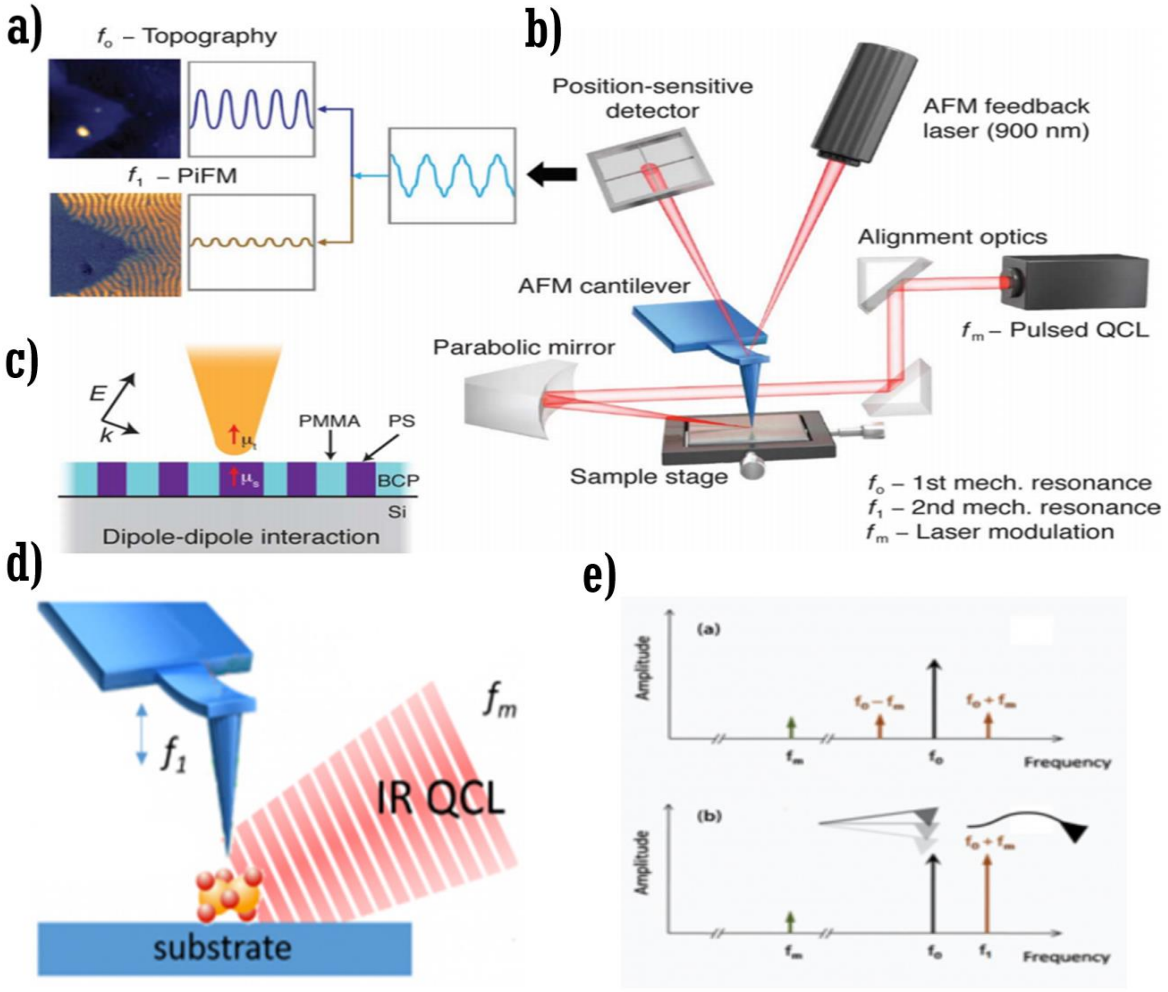

Figure 11 Different Detection schemes in PiFM [8]

Here in this Figure 11, a) Topography with f_o frequency and PiFM signal with f_1 eigenmode. b) Working principle of PiFM using tunable laser c) Dipole-Dipole Interaction. d) Sideband mode using $f_1 = f_o + f_m$ where f_m is laser frequency. e) Sideband and Direct mode presentation using all three different frequencies. [11]

4. Convolution effects

This chapter contains a study on convolution effects in AFM topography.

Atomic force microscopy deals with tip-sample interaction and manages topography images to raise awareness of the sample surface. As discussed, the AFM tip would work uniquely for achieving better outcomes than any other optical instrument. Our aim is to do further development of analysis routines and understanding for biomedical application. Therefore, we have used different samples to test like polymer films, nanoparticles, biochemicals, bacteria, and biomedical tissue (human retina). Every material has its surface roughness characteristics and varies concerning its requirements to implementations. In this project, the nature of AFM tip convolution is to be studied and followed by their deconvolution methods. [5][22]

This project aims maximum topography data extraction and needs to be achieved by initially conceptual theories of PiFM and its significant components.

AFM, like any other measurement technique, is prone to artefacts. The artefacts can arise due to AFM Probe, the scanner, the instrument electronics, lab ambient, user familiarity. In AFM Imaging, these artefacts are sometimes easy to spot irrelatively its awareness by a user. Though more artefacts can be avoided if a user knows their source, many hidden artefacts cannot be avoided.

4.1 Probe Artefacts

Probe artefacts are the most commonly seen in the PiFM (or in AFM). AFM images are a convolution of the topography of the sample with the shape of the tip. When analyzing AFM pictures, we often assume that the tip radius is less than the details seen and that the probe's opening angle is smaller than the sample's features. There are also a few difficulties that users would face after using the same tip for a longer time, and with many readings, it may get blunt or contaminated. Continual use of the tip also leads to decreasing life of reusability.

There are found some common effects on the tip [2]:

1**.** Too large features are imaged

2**.** Holes are imaged small

3**.** Repetition of features is imaged

4. Strange Shapes are imaged.

4.1.1 Blunt probes

Typically, blunt probes provide pictures with larger-than-expected features and a flattened profile, as shown below. Holes on a flat surface would seem more minor when probed with blunt probes than when probed with sharp probes [2]

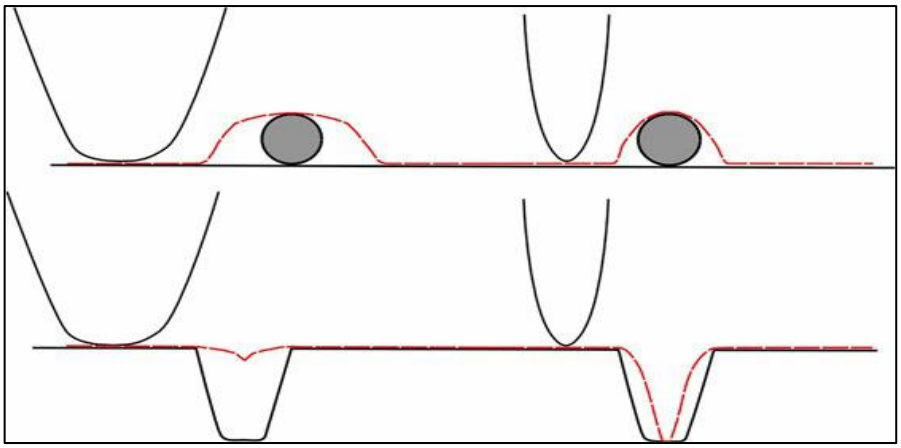

Figure 12 Blunt Probe Schematic Presentation [2]

Here, it can be said that dilation is a typical feature of the force imaging process. For instance, measurement of rounded contours with a known diameter of 2 nm would create a mess of an additional 10-20 nm width. It can be understood graphically from Figure 12. Having this kind of convolution once or a few more times is a regular feature, but it changes its appearance significantly when it happens quite often during a scan. At this moment, changing a probe is recommended.

4.1.2 Contaminated or broken probes

Contamination is a widespread problem in AFM imaging. It leads to more dirty probes than any other factor. Biological and different soft samples and any sample with loose particles on the surface contaminate probe tips rapidly, resulting in image deterioration. Broken tips are not a very common problem, but they also occur when the probe scans the sample outside feedback loop control. Using both kinds of probes would result in unexpected sample shapes and repeating patterns within the images. In the below Figure 13, more details are demonstrated.

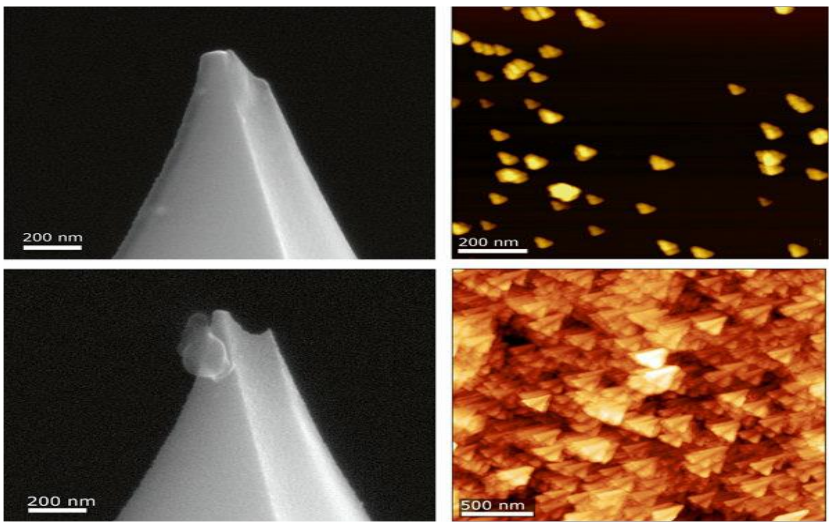

Figure 13 Left: SEM Photos of Broken and Dirty tips and Right: their AFM results[2]

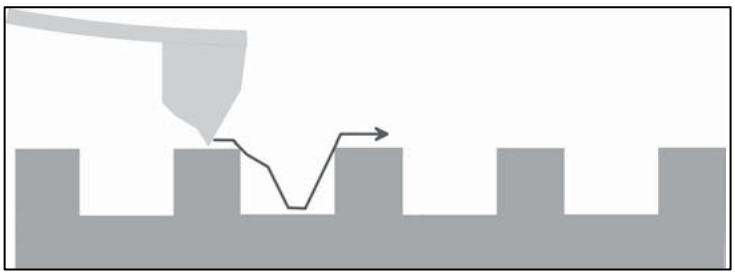

Figure 14 Damaged tip effects artefacts [2]

4.1.3 Double tips

In this case, if the tip breaks itself so that it creates multiple spikes at its peak. Unwanted debris gathered at the end of the tip also works as a double tip and consequently result in repeating patterns in the AFM images. In such effects, there are 'true' and 'acquired' tip that scan the surface.

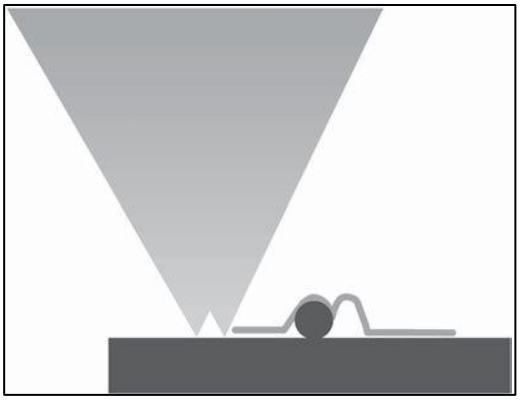

Figure 15 Double tip causes a shadow or double image[2]

4.1.4 Miscellaneous unwanted tips effects

Artefacts may be created while scanning significant features, as shown in Figure 17, because of the considerable angle that the probe is at with the material. This angle places the AFM probe in a position where it is perpendicular to the material's surface. The probe–sample angle cannot be adjusted mechanically on certain AFMs. Three adjustment screws are often used to alter this angle.

Secondly, because of the difficulty in adequately imaging some samples (in Figure 16), particularly those with very high aspect ratios, a picture may include repeated images of the probe or its sidewalls.[2]

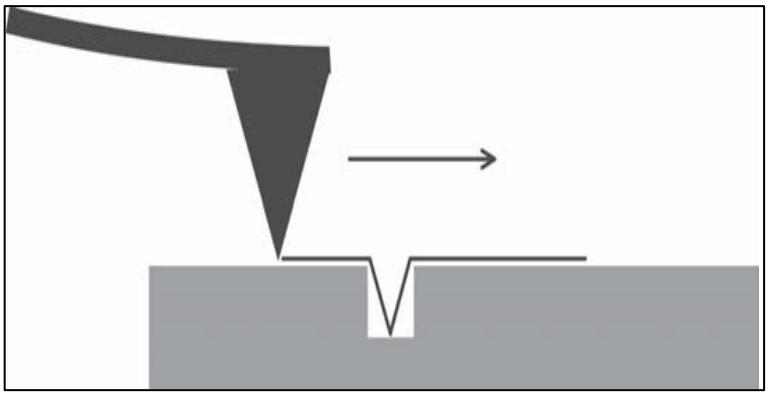

Figure 16 The hole cannot be reproduced because of the width of the tip[2]

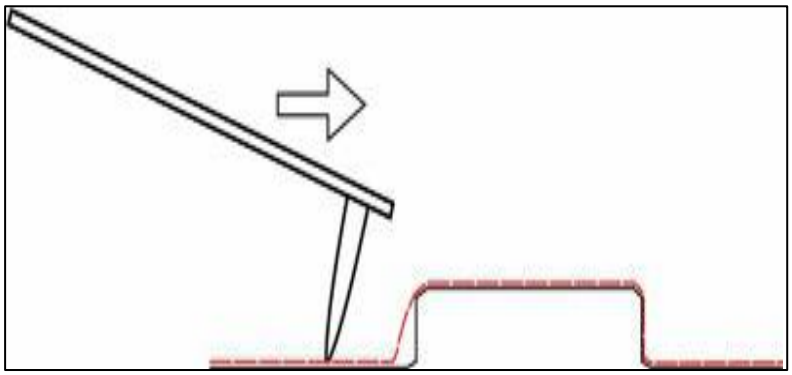

Figure 17 A schematic representation of probe–sample angle issues. Distortions occur when the probe is angled concerning the sample, and sample characteristics look asymmetrical.[2]

5. Deconvolution Methods

In Atomic force microscopy, using a piezoelectric scanner and a z-feedback loop, an AFM tip may be brought to within nanometres of a sample's surface and maintained there, as described in "2 State of the Art". All potential forces between the tip and the sample are added along with the tip's physical structure and across a small area of the sample's surface to produce the tip-sample interaction in AFM. Because of these influences, the information that depicts a particular feature of the sample surface may be distorted. In the form of physically ignored area information, any tip shape produces particularly problematic artefacts.

The modelling and characterization of the tip and sample artefacts in future deconvolution techniques are essential for AFM data processing. When the sample surface has sharp nanoscale features, the surface measured by the AFM may be understood as the sample convolution with a transfer function whose characteristics depend on the tip's parameters when modelling the AFM data as the output of a continuous-time system. A linear deconvolution of the measured surface may recreate the actual image once the tip characteristics are precisely known. The scanning tip's apex and aspect ratio are two significant factors of AFM resolution.[23]

This chapter examines and compares deconvolution techniques. They are primarily concerned with eradicating irregularities from the recorded pictures. Since convolution effects have been described before, the tip plays a significant role in creating a convolution in the frame and removing missing or unnecessary information from the surface. These proposed approaches are primarily concerned with the geometry of the tip, with other influencing variables coming second.

AFM image contains various depressions and heights. Each one of them would rise to particular artefacts. Any AFM image containing an undefined force microscopy image is constrained by morphological restrictions that are fundamental in the imaging process. Morphological constraints limit various tip shapes, and AFM images are taken using those tips. It can be said that morphological constraints affect the AFM output. The convolution effect explained in chapter 4 caused by broad tips could not create narrow contours. This morphology method usually sets an utmost limit for every kind of feature in images. The morphology method takes every point in the image and defines a bounding surface for each point, respectively. This method creates a surface reconstruction without knowing the actual tip. The actual tip would be the same size or smaller than the largest tip that meets all requirements. If there are sharp features in the image, this method could estimate a more accurate tip shape, and once the tip shape is known, it can be simulated over the surface, and reconstruction can be expected. Dilation and erosion have been introduced to derive mathematical explanations. Dilation adds the pixels to the image, and erosion removes the pixel. Following methods like tip geometry method, mirror tip creation method, mathematical model for different objects shapes work using tip geometry and software packages explained later on this chapter derives its from morphological method (Like Gwyddion and SSIP).

5.1 Method of Tip Geometry

This method was carried out by Peter Markiewicz and M. Cynthia Goh in 1995. [13]

The authors present an algorithm for deconvolution of the probe tips used with the atomic force microscope from images of calibration grids created using very large-scale integrated technology. One such algorithm helps visualize the tip before or after visualizing to explain the tip's condition. This technique is universally applicable: it estimates the tip geometry and does not require any data preparation, including filtration. Grids with circular depressions represent circular and conical tips' geometries correctly but have constraints when imaging square pyramidal tips. The precision of tip reconstruction is restricted by slight changes in the size and form of depressions within a geometric pattern.

5.1.1 Methodology

Typically, a convolutional mess occurs as a result of tip and sample roughness. Deconvolution has been arranged in this way solely in terms of tips. Typically, the tip is discovered blunt or distorted during the AFM scan.

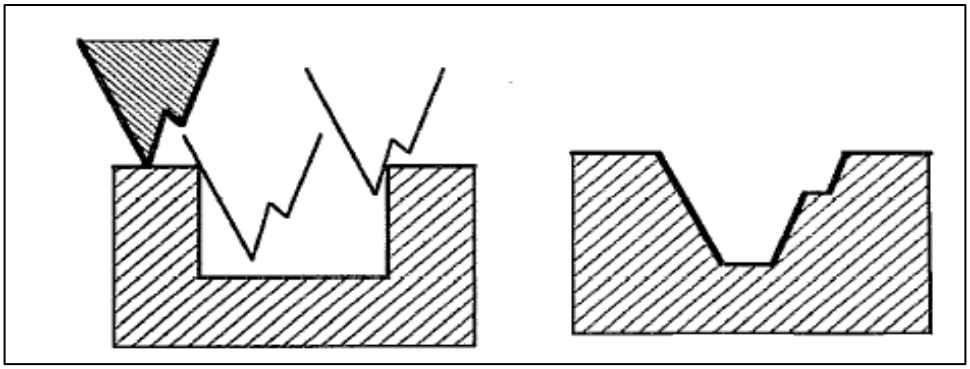

Figure 18 Left: Movement of the tip on the surface having a finite depression and right: Investigated shape of the tip cropped on original surface depression[13]

The convolution procedure is illustrated in Figure 18 for a two-dimensional model of a sample depression and a triangle tip with a minor imperfection. As the tip travels over the flat upper section of the sample, contact is made only at the apex until the tip reaches the rim, at which point contact is made along the tip's face. Once the tip reaches the bottom of the depression or crosses entirely over the opposite edge, the connection is re-established at its apex.

The regime in which the contact is not at the tip's apex is crucial because the AFM image is reconstructed using this assumption, resulting in the picture depicted by the heavy profile in Figure 18 for the model investigated. As can be observed, the left shape of the tip is mirrored in the depression's left-hand half, while the right profile with the notch is reflected in the opposite area. An investigated model of any surface depression is defined as the point-to-point monitor of the tip motion. The tip apex could not reach each point of the surface irrespective of its geometry. Thus, it can catch only

those points that are in its way of scan or touched by an adjacent tip wall. These all points design a complex shape.

The image is a convolution of the tip and the sample, and the extent to which the tip part dominates the image is dependent on the tip's relative size to the depression. The proposed method was utilized to generate the tip geometry's design or shape. The method's purpose is to replicate the convoluted tip's geometry. Other unknown deconvolutions of the surface could be achieved using this geometry. This method is recommended for universal inputs, although some drawbacks have been discovered. Still, different characters are often used.

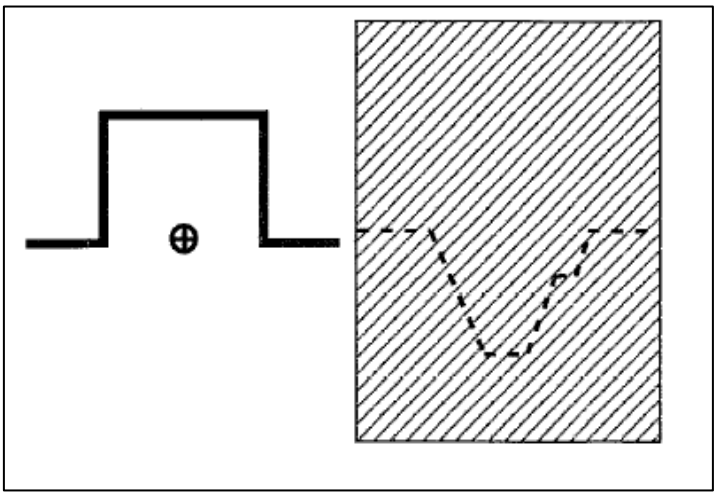

Figure 19 Mask being brought to the surface and creating a tip geometry [13]

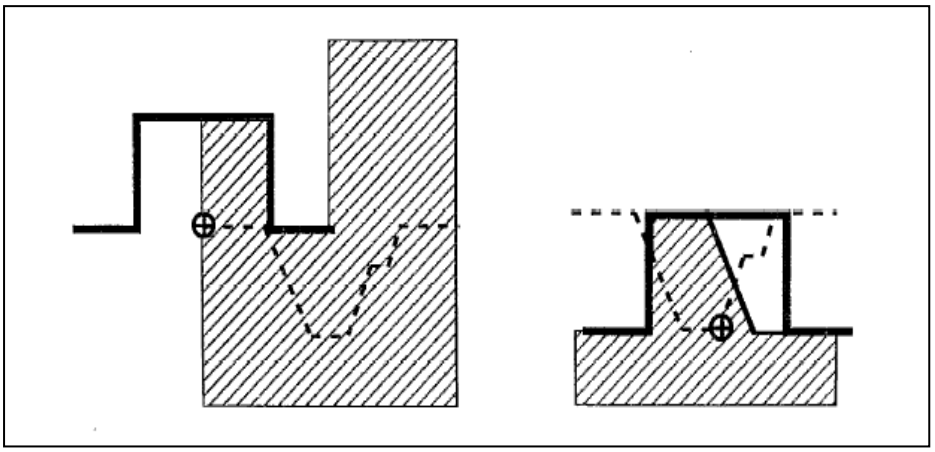

Figure 20 Schematic Diagram of a moving mask onto the surface [13]

In Figure 19, the next step is to cover a mask on the investigated model. It proceeds with the computation of a mask shaped like the opening, inverted, and with the correct diameter. The mask is constructed so that every sample data point of a height lower than that of the mask is kept unchanged, while those higher than this field are reduced to the value of the mask.

After the mask is covered, the next step is to extract the tip's geometry. This is for what mask is created. Here, it is noted that depressions with extremely steep walls do not have to be fully modelled; a simplified representation of the depression that addresses its opening is available. This is beneficial for deconvolution images with slightly angled samples or where the actual depth of the depression is undervalued. The midpoint is situated at the inverted surface for levelled sample photos, corresponding to the baseline illustrated in Figure 19. A skewed baseline would be required to account for slightly slanted photos.

In this step, the program next creates a sample "block," All topographic data are adjusted to their highest value for a scan size identical to that of the AFM picture, as illustrated in Figure 19. This illustration can be understood from Figure 20 & Figure 21. This movement needs (in Figure 20) to be carried out so that block passes through every point of the wall of the investigated model. The final sample profile is fully processed, and a faithful copy of the tip shape is shown in Figure 21.

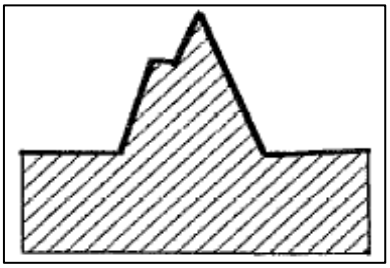

Figure 21 Tip Geometry created from a mask movement on the investigated surface[13]

5.1.2 Practical Realization

In this study, Equipment's and data obtained from the experiment by Marckiewicz and his colleague are below:

An array of circular VLSI depressions was imaged using a variety of tips. The Nanoscope II was used in contact mode to collect data (Digital Instruments). All photographs were taken in the height mode with a gain setting of 2 for integral and 3 for proportional gain. Typical working forces were in the neighbourhood of 100 nN, and scan speeds were less than 2 Hz. Accompanying photos taken in the force mode, which represents the cantilever's deflection from the set-point, revealed minor fluctuations at these values.

As discussed earlier, this method has also been experimented with physically. In Figure 22, the same has been exhibited. This has been carried out using three different types of AFM tips.

[1] Square Pyramidal Tip
[2] An Ultra lever Tip (Park Scientific)
[3] A Blunted Tip

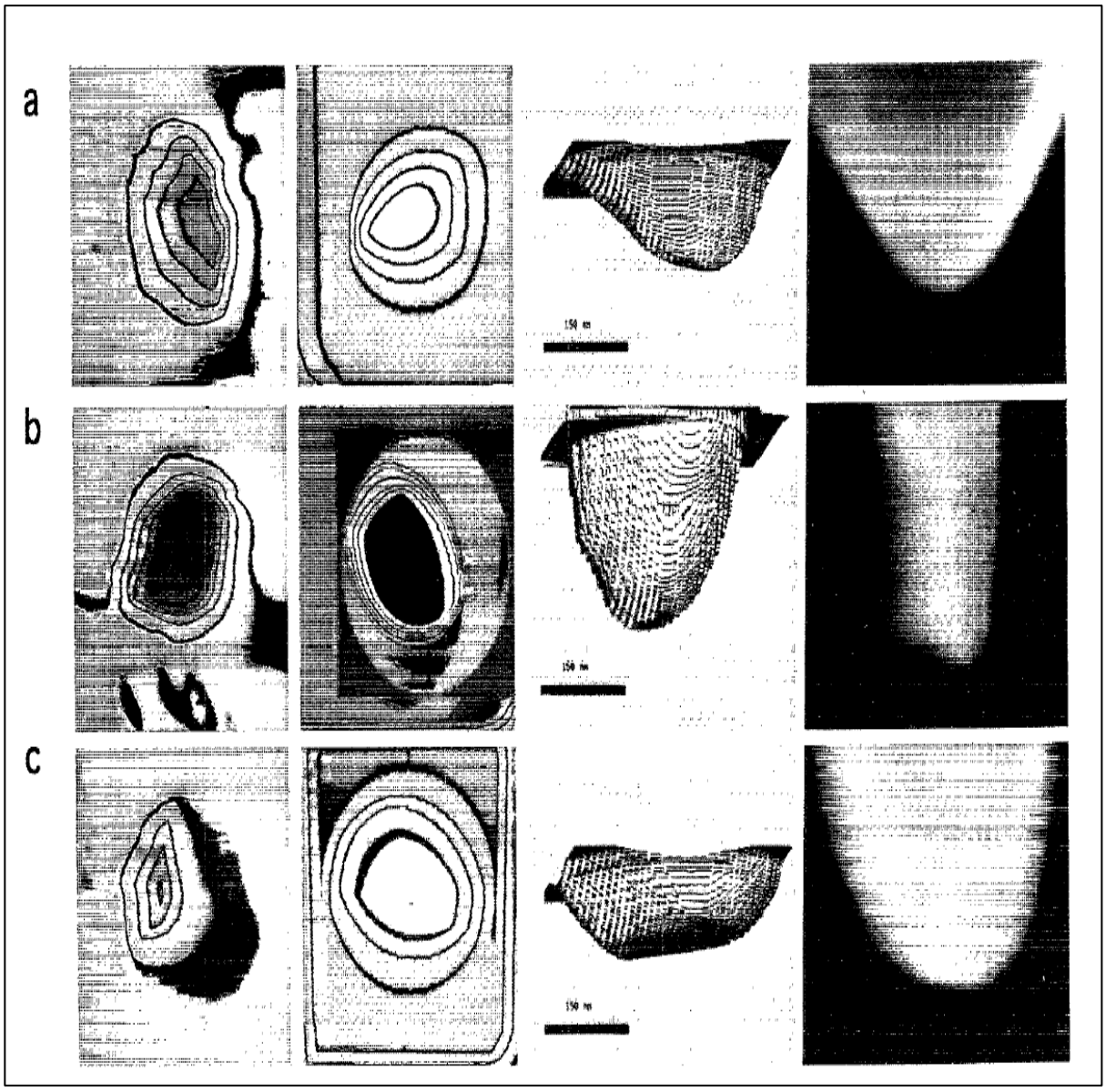

Figure 22 Deconvoluted results (a) a standard square pyramidal tip, (b) an Ultralever tip, and (c) a blunted Ultralever tip. [13]

The first column of Figure 22 shows the raw AFM images, with contour lines spaced approximately 25 nm apart. The number of contour lines indicates that two of the points [Figure 22(a) and Figure 22(c)] penetrate approximately 75nm into the depressions, failing to reach the bottom due to their high radius of curvature and low aspect ratio. The sharp Ultra lever makes a deeper penetration into the depression. Due to the inability to thoroughly probe the holes, the tip geometry reconstructed using the deconvolution technique is limited. To gather the most information about the tip geometry, it is necessary to use a hole with a big diameter and depth.

The second column of Figure 22 displays the deconvolution findings for each tip using an ideal circular mask with a diameter of 405 nm. As previously stated, the deconvoluted images for the square pyramidal and blunted tips reveal these

geometries only to a height of 75 nm due to the high curvature radii limiting the amount of material that penetrated the depressions. Only the Ultra lever was capable of reaching the 200 nm depth in this case. The third column of Figure 22 compares these deconvoluted pictures seen at an oblique angle to the scanning electron micrographs of the tips in the fourth column.

The outcomes for the square pyramidal tip are unsatisfactory. It is possible to demonstrate that the tip's rounded facets reflect the curvature of the grid depression. While passing through the circular grid apertures, the square tip only touches the tip body's edges. Only those areas of the tip that contact the calibration standard are faithfully recreated from the deconvolution of AFM data. In contrast, those that never made touch are occluded, as previously stated for spherical calibration standards.

Thus, a minor crack or any portion of the tip with a radius of curvature more significant than the standard will not be precisely recreated with the standard's curvature. As a result, circular grids are inadequate standards for deconvolution of square pyramidal tips. The AFM-deconvoluted images of the tips are slightly larger than the SEM-deconvoluted images.

5.2 Inverted Tip Method

This method was carried out by A.A. Bukharaev, N.V. Berdunov, D.V. Ovchinnikov and K.M. Salikhov in 1997.[9]

Atomic force microscope (AFM) pictures frequently contain distortions induced by the tip and sample surface converging. The proposed numerical deconvolution method, which employs an inverted tip at a fixed height above the surface, significantly varies from previously reported methods and is essentially straightforward to implement in practice. This approach was successfully utilized to extract the shape of the AFM square pyramidal tip using nanometer-sized spheres. Once the rebuilt AFM tip shape was combined with a deconvolution process, accurate structures of the circular 90 nm sized particles were generated.

The deconvolution algorithm's simplicity and relative speed are determinants of its usefulness. It is also critical to consider the similarity of the deconvoluted surface picture to the actual topography. Additionally, the method should be adaptable to various shaped tips and surfaces and associated AFM pictures. Most surface reconstruction methods are based on the search for the coordinates of the tip's actual point of contact with the examined surface.

The approach of computer deconvolution is examined in this article to reconstruct the form of the AFM tip and further improve the AFM picture of the researched surfaces.

5.2.1 Methodology

Here, the deconvolution approach searches for the coordinates of the tip's real contact locations with the surface throughout the scanning operation. The process of two-dimensional modelling of an image acquired with an atomic force microscope in contact mode is illustrated in Figure 23.

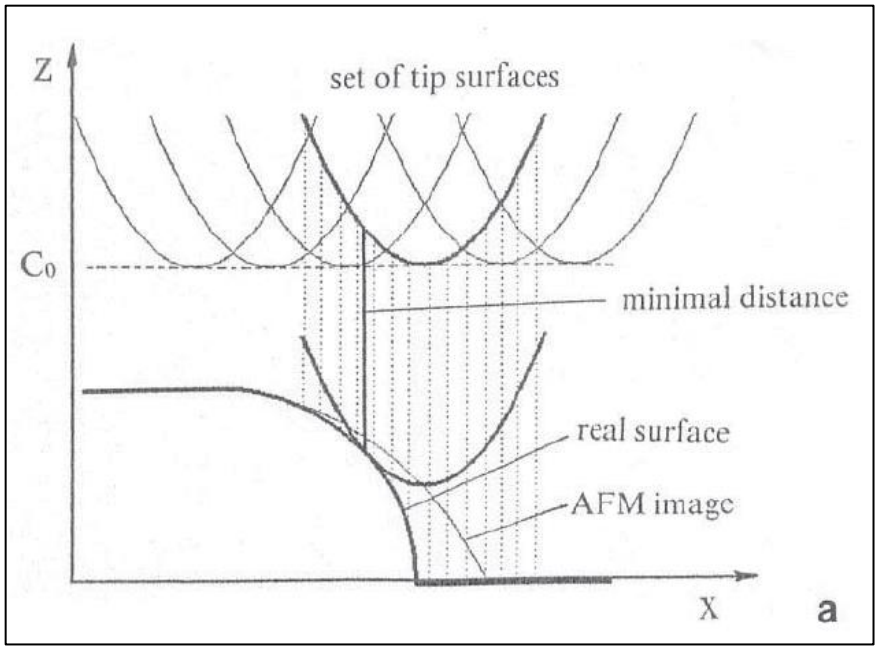

Figure 23 2D Simulation of AFM Imaging on the surface contours [9]

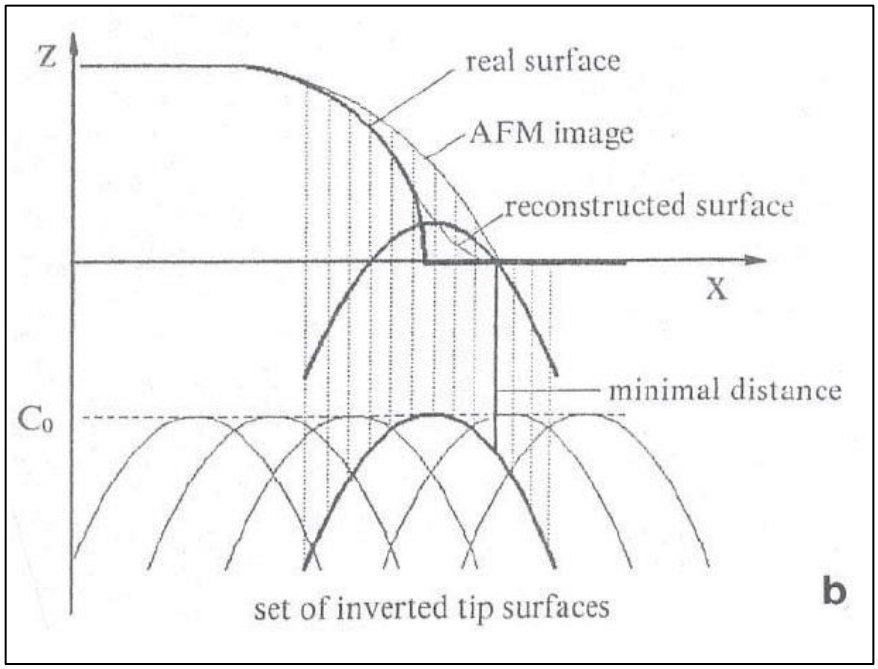

Figure 24 2D Simulation using invert tip and getting a reconstructed surface [9]

The tip specified by the function T(x) with the top at x = 0, i.e. $T(0) = 0$, is placed at a constant height C_0 above the surface. Then horizontally, one step at a time, the point is displaced along the surface in this manner. That its height C_0 remains constant at all times. The tip position at its apex and point x_0 is defined as:

$$T'(x,x_0) = T(x-x_0)+C_0 \quad (1)$$

Following each displacement, the exhaustive search determines the shortest distance along the z-axis from the tip profile $T'(x, x_0)$ to the sample surface $S(x)$.

$$h(x_0) = \min_x \{T'(x,x_0)-S(x)\} \quad (2)$$

The tip is brought into contact with the surface by this measure.

$$T''(x,x_0) = T(x-x_0)+C_0-h(x_0) \quad (3)$$

This is a lot like the scanning process in real life. Consequently, due to such displacements, the tip's top (or another fixed tip point) will trace the trajectory corresponding to the visible AFM picture.

$$I(x_0) = C_0-h(x_0) \quad (4)$$

After completing a similar method with the image I(x) acquired earlier, the surface $Z(x)$ can be generated (Figure 24) by employing an inverted tip $T_{inv}(x) = -T(-x)$, which is kept at a constant distance but is already positioned under the picture profile $I(x)$. Except for the locations where the scanning tip did not contact the surface (the "black holes" areas), $Z(x)$ is identical to the actual surface. The basic concept behind our deconvolution process is the use of an inverted tip profile.

Figure 26 depicts the two-dimensional case's convolution/deconvolution procedure. Because of the point x*, tangency equations describe the convolution process when the tip comes into contact with the surface.

$$\frac{\delta S(x)}{\delta x}\Big|_{x=x^*} = \frac{\delta T''(x)}{\delta x}\Big|_{x=x^*} = \frac{\delta T(x)}{\delta x}\Big|_{x=x^*} \quad (5)$$

$$S(x)\Big|_{x=x^*} = T(x - x_0)\Big|_{x=x^*} + I(x_0) \quad (6)$$

In this Figure 25, convolution and deconvolution have been carried out and shown. As convolution equations are built, the same way deconvolution can also be generated.

$$\frac{\delta I(x)}{\delta x}\Big|_{\underline{x}=\bar{\underline{x}}^*} = \frac{\delta T_{\underline{inv}}''(x)}{\delta x}\Big|_{\underline{x}=\bar{\underline{x}}^*} = \frac{\delta T_{\underline{inv}}(x)}{\delta x}\Big|_{\underline{x}=\bar{\underline{x}}^*} \quad (7)$$

$$Z(\bar{x}_0) = T(\bar{x}_0 - x)\Big|_{\underline{x}=\bar{\underline{x}}^*} + I(x)\Big|_{\underline{x}=\bar{\underline{x}}^*} \quad (8)$$

Furthermore, consequently, the condition of the tip is defined as:

$$I(x)\Big|_{\underline{x}=\bar{\underline{x}}^*} = T_{\underline{inv}}(x - \bar{x}_0)\Big|_{\underline{x}=\bar{\underline{x}}^*} + Z(\bar{x}_0) \quad (9)$$

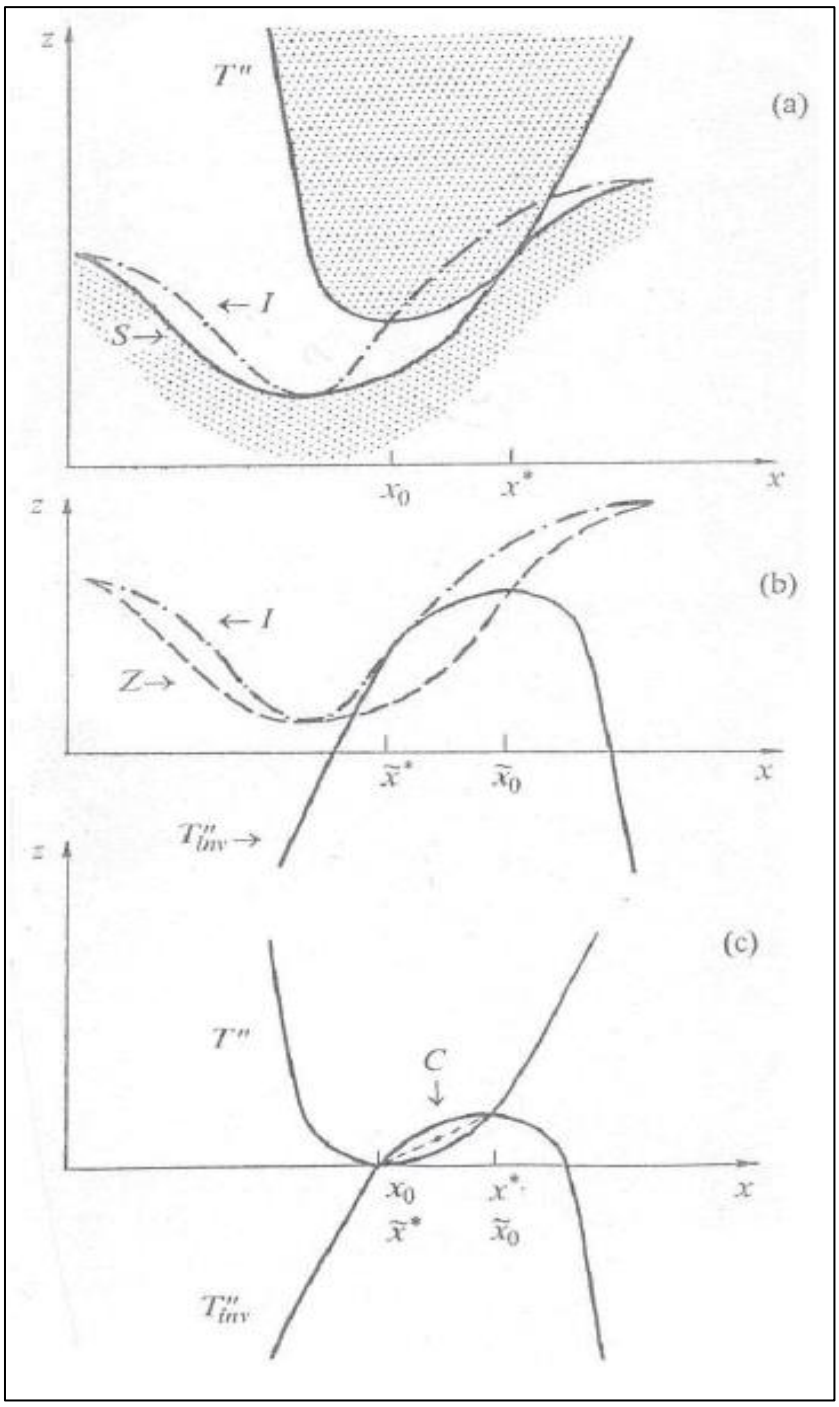

Figure 25 2D Simulation of AFM (a) and deconvolution (b) process. (c) Presentation of the intersection of the inverted and initial tips. [9]

From this schematic presentation and mathematical calculations, it can be said that the deconvolution algorithm is nothing but a convolution of acquired AFM output and the inverted tip.

Figure 25(c) demonstrates the equivalence $Z(x) = S(x)$, where C denotes the inversion centre. Equations 6 and 9 are identical if and only if the criteria $\bar{x}_0 = x^*$ and $x_0 = \bar{x}^*$ are met concurrently. Under the inversion qualities, these prerequisites are met. Indeed, if we set the top (maximum) of the inverted tip curve $T_{inv}''(x)$ to the point x*, and so satisfy

the condition $\bar{x}_0 = x^*$, the inverted tip curve $T_{inv}''(x)$ will cross the initial tip curve T''(x) at x_0. Due to the inversion properties, this point's coordinates correspond with the contact point between the inverted tip and the AFM image $I(x)$, which is why $x_0 = \bar{x}^*$

At all contact sites between the inverted tip and the surface image, these conditions will hold. As a result, Equations (6) and (9) are similar, and $Z(x)$ equals $S(x)$. As demonstrated via numerical simulations, this is also true for three-dimensional deconvolution.

The computer simulation of a complete reconstruction of the authentic surface image is depicted in Figure 26. Other surface structures where the AFM tip does not contact all surface locations (Figure 26(Right)) show partial reconstruction. Additional refinements to the deconvolution algorithm will undoubtedly enable delineating "black hole" locations on partially reconstructed images.

The equations above follow that using the identical deconvolution process on a test sample with known surface geometric parameters can recreate the utilized tip shape from the AFM image.

5.2.2 Practical Realization

The experimental AFM pictures were acquired using the commercial scanning probe microscope P4-SPM in contact mode. A laser beam reflected off the cantilever's backside was used to detect the tiniest touch between the tip and the surface. A differential signal amplified from a four-section photodiode enables the determination of the cantilever's angular deflection with an accuracy of up to 0.1", corresponding to a resolution of 0.1 nm. The scanning was performed with the feedback turned on, and the standard operating force was around 10 nN in this scenario. Park Scientific Instruments' probe tips were composed of silicon nitride and had a square pyramidal form.

On a silicon and mica substrate, nano-sized latex spheres were deposited. They were utilized to evaluate this deconvolution technique and compare experimental and computer-simulated AFM pictures obtained before and after an AFM operation.

Figure 26 depicts a computer simulation of tip shape reconstruction utilizing a known-sized hemisphere positioned on the test sample's surface. The example demonstrates that calibrated spherical fine particles are an excellent test sample for reconstructing the three-dimensional AFM tip apex.

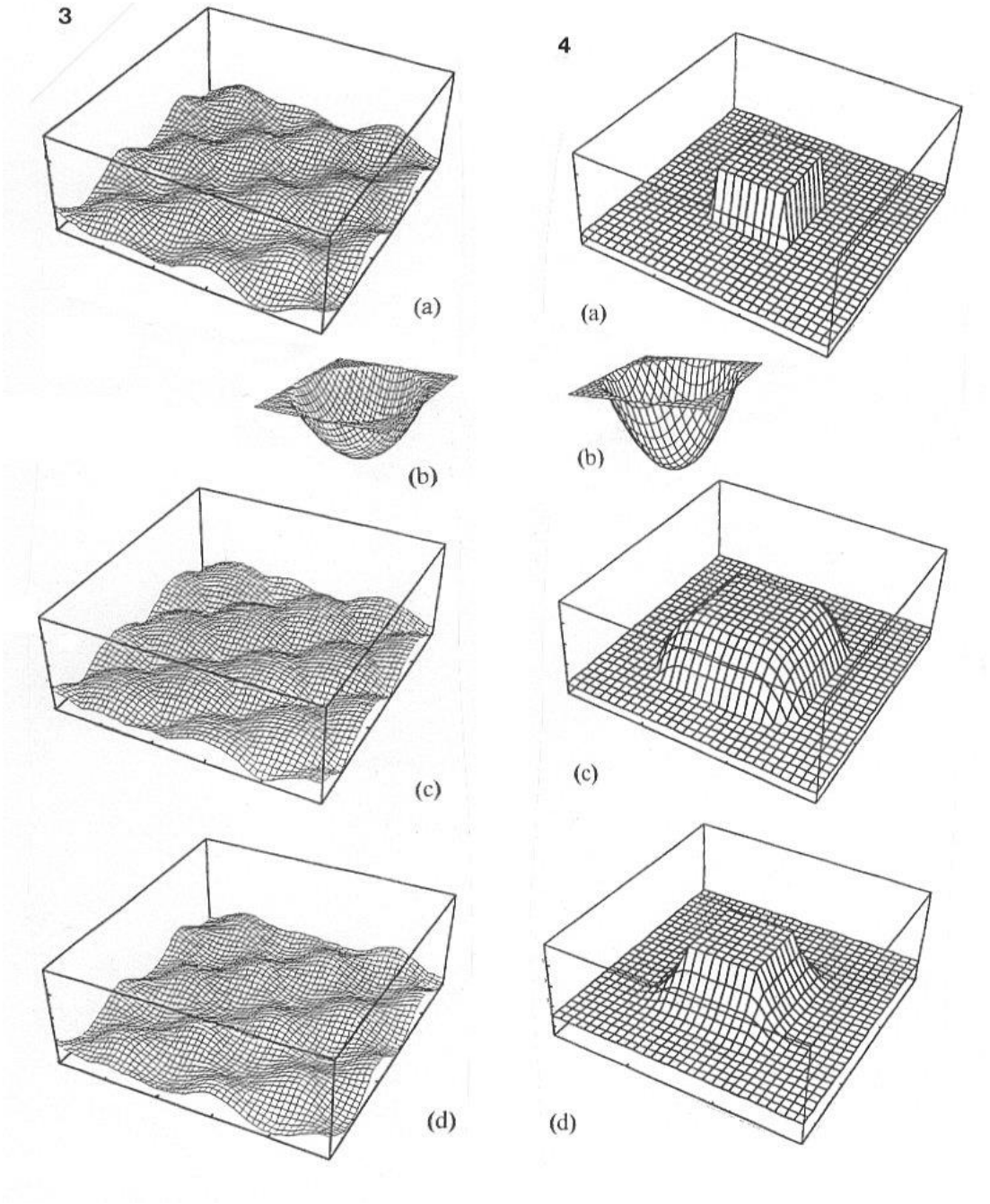

Figure 26 3D Simulation of (left) actual surface reconstruction using deconvolution (right) square protrusion partly reconstruction where (a) Initial True surface (b) Probe Surface (c) AFM Image surface (d) Reconstructed image surface [9]

A gold covering with a thickness of 20 nm was employed to stabilize the tiny particles on the surface.

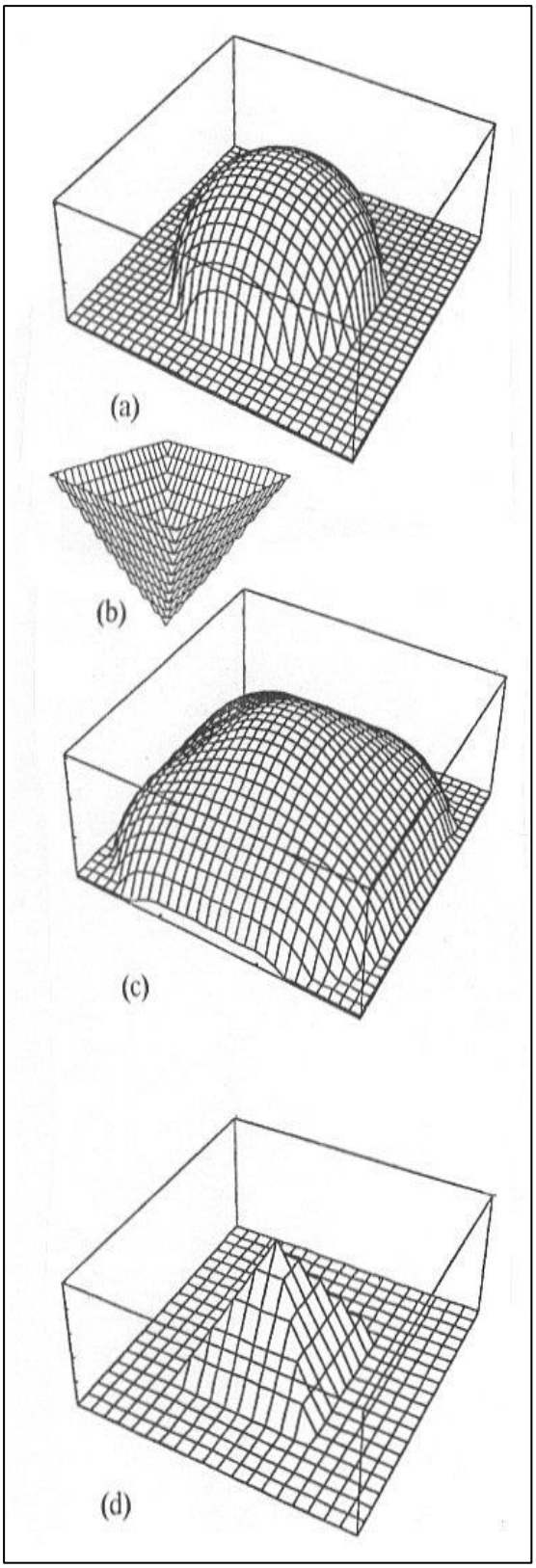

Figure 27 3D computed simulation of extraction of the pyramidal tip shape for sphere protrusion using deconvolution shape. Here (a) True half-sphere shape (b) tip image (c) convoluted sphere image (d) Extracted tip shape [9]

5.3 Mathematical Method

This method is carried out by Josep Canet-Ferrer, Eugenio Coronado, Alicia Forment-Aliaga and Elena Pinilla-Cienfuegos in 2014.[10]

As described in this method, *"The convolution error rises with object height, most notably for tiny motifs. Between rectangular and elliptical objects of the same size, there is some significance of the object form. These variations are to be expected among elongated things but diminish as the aspect ratio of the item increases."*

The procedure used in this investigation was used to investigate the dimensions, shapes, and aspect ratios of various nanometric motifs on a flat substrate in this work. Indeed, this technique allows for the extension of convolution artefacts to any theme, including actual surface roughness.

5.3.1 Methodology

Convolution occurs due to a multitude of factors in AFM. A tip from them is critical in causing AFM to be impacted by convolution. During a scan, the tip and surface have a significant effect on the primary artefacts. Canet Ferrer and his colleagues developed a compelling mathematical model that describes the convolution effect from its inception through its deconvolution.

3D simulation can also be conducted with ordered matrices, although it requires more computing capacity. However, it may be helpful in future studies because it allows complete AFM imaging simulation. In any instance, AFM image profiles are used to evaluate quantitative AFM data. The AFM tip is illustrated to demonstrate some of the geometrical elements of this type of simulation. As with earlier research, the probe is represented as a circular apex cone. As will be demonstrated below, these settings have the most influence on the tip convolution effects. Down, the same overview is carried out.

The following terminology is used:

C as a first contact point, C' as a substrate contact point, h_{eff} as the effective height of the object, W_{eff} as the object's width, r_{tip} as tip radius and γ as a tip to face angle are described. Additionally, identifying L and T as the object's leftmost and topmost points will aid future discussion.

The convolution effects at the tips are quantified using the difference between the measured width (W_{exp}) and the actual width (W_1, which is a simulation input) derived from profiles in 2D simulations (Convolution = W_{exp} - W). The influence of the surface motif on simulations of 2D rectangular and elliptical objects is studied. With these results, we can discuss the role of various parameters in the tip-convolution phenomenon. The importance of object height is demonstrated by comparing simulation profiles for objects of multiple sizes. In contrast, the results of different scanning shapes are shown by comparing rectangular and elliptical motifs. Finally, the impacts of the tip parameters are investigated by running the simulations for a wide range of r_{tip} and γ.

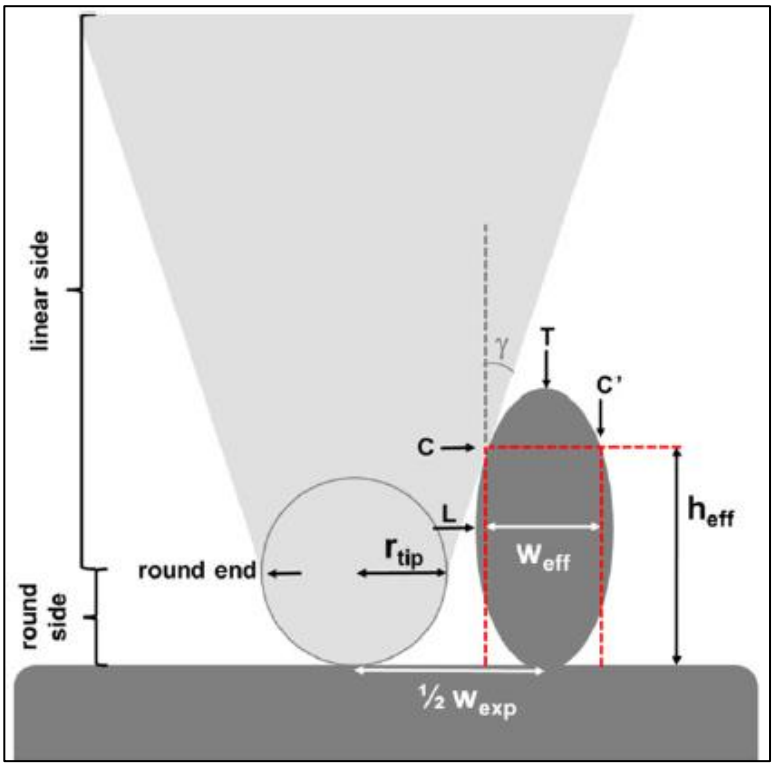

Figure 28 Geometrical representation of tip standards and object standards [10]

5.3.2 Results & Discussion

Convolution effects on AFM topography data are known to be sensitive to h and object geometry. The ratio of h to w is defined in this work as the aspect ratio, A = h/w. The addition of this parameter will enable us to discriminate between the inputs of height and shape to the convolution distortion. Our analysis contains a review of the basic concepts behind convolution effects as explored via geometrical considerations. Four specific examples are presented in detail to demonstrate how shape and height affect convolution shortcomings. Each situation features a different size and form of the tip. Tip size and object shape are of importance to each other in the creation of a convoluted mess, as previously described. In the Diagram below, convolution Δ is the

referred-to object. It can be interpreted as real and effective being distinct concepts. When the tip round contacts the object before it should, it results in a sloppy convolution. The magnitude of convolution is measured using geometric techniques and notions.

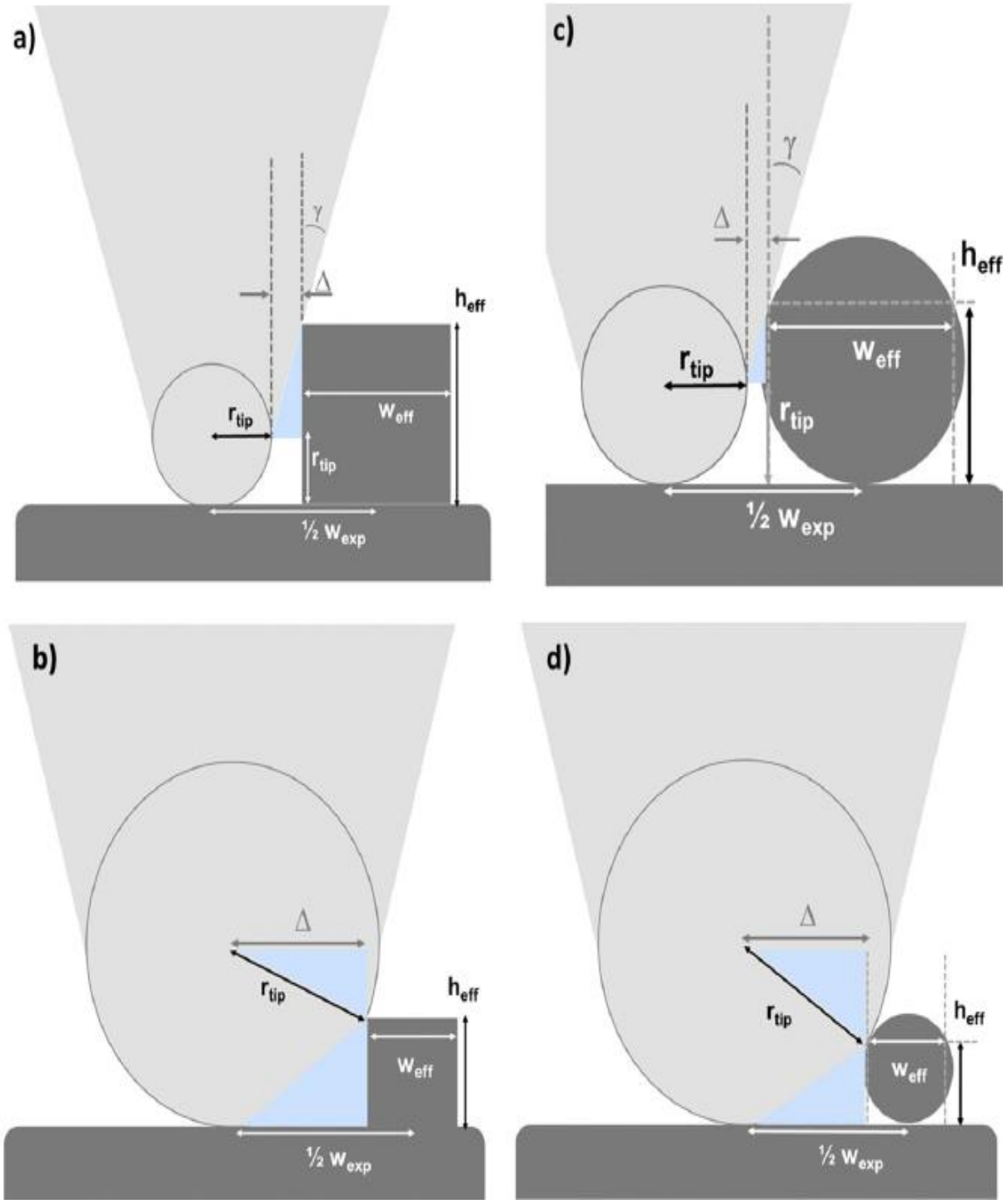

Figure 29 Schematic Diagrams for tip convolution and trigonometric consideration of (a) & (b) Rectangular objects and (c) & (d) Circular Objects [10]

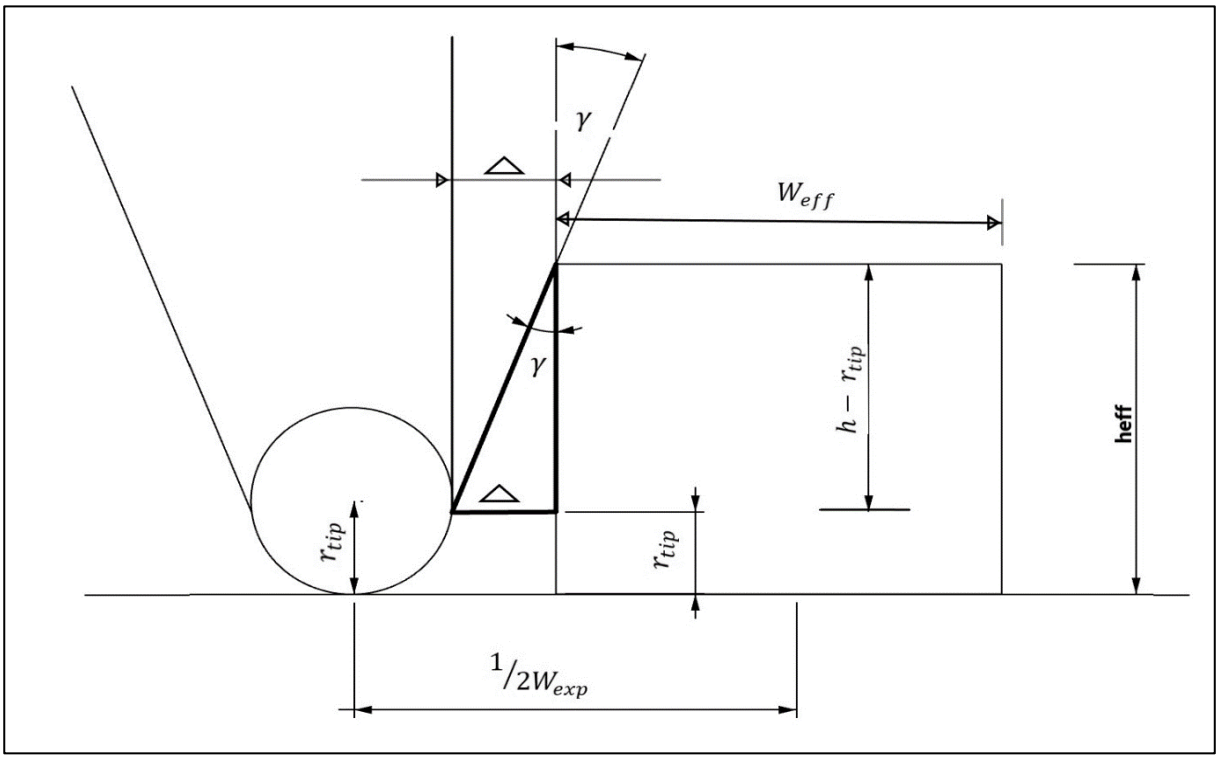

Figure 30 Schematic Diagram of a case a, getting tiny geometrical data showing actual height and image height.

As seen in instance (a), the round tip is smaller than the item, and the object is rectangular. Additionally, the term "convolution" is used. A convolution triangle (highlighted in black) is assumed, and specific geometrical calculations are carried out within it.

Since the tip radius is less than the effective height of the item, the contact point would be at the object's top-left corner. So, we can get the part of the W_{exp} as:

$$^1/_2\, W_{exp} = r_{tip} + \Delta + {}^1/_2\, W_{eff} \quad (10)$$

$$\Delta = \left(h - r_{tip}\right) tan(\gamma) \quad (11)$$

From the given terminology, the given geometrical calculation can be carried out. If the consideration as h >> $2r_{tip}$ assumed, the convolution would be $2h\ tan(\gamma)$. In this case of convolution effect, point C is above the round tip centre. This can be suggested here that when point C is measured above the round tip shape, convolution gets affected into the AFM image irrespective of the radius of the tip r_{tip}.

Case a	Referring to C at the tip's linear side area (h > r_{tip}); a rectangular-shaped object
Equation	$^1/_2\, W_{exp} = r_{tip} + \Delta + {}^1/_2\, W_{exp}$ $\Delta = (h - r_{tip})\, tan(\gamma)$
Height-to-tip correlation	$\mathrm{h} = 2\mathrm{r_{tip}}$
Position of C	C is above concerning tip round centre
Convolution	$\Delta = 2h\, tan(\gamma)$

Table 1 Geometrical calculation of convolution when the object is rectangular and Point C above the tip round centre

Explaining scenario b, when the object height is significantly less than the tip radius, revealed that the contact point is mainly located below the tip circle centre. Convolution is also assessed here. In this case, the following geometrical data can also be achieved:

$$^1/_2\, W_{exp} = \Delta + {}^1/_2\, W_{eff} \qquad 12$$

Moreover, the using angle co- relation inside convolution triangle, the nearby value of convolution can be calculated as:

$$\Delta = r_{tip}\, Cos \left\{ ArcSin \left[{}^{(r_{tip} - h)}/_{r_{tip}} \right] \right\} \qquad 13$$

In this situation, the h = 2r tip was discovered. Point C is also measured below the round tip end, indicating that convolution (r_{tip}) is now impacted solely by the tip radius. Using these assumptions, convolution is measured as:

$$\Delta \backsim r_{tip} \qquad 14$$

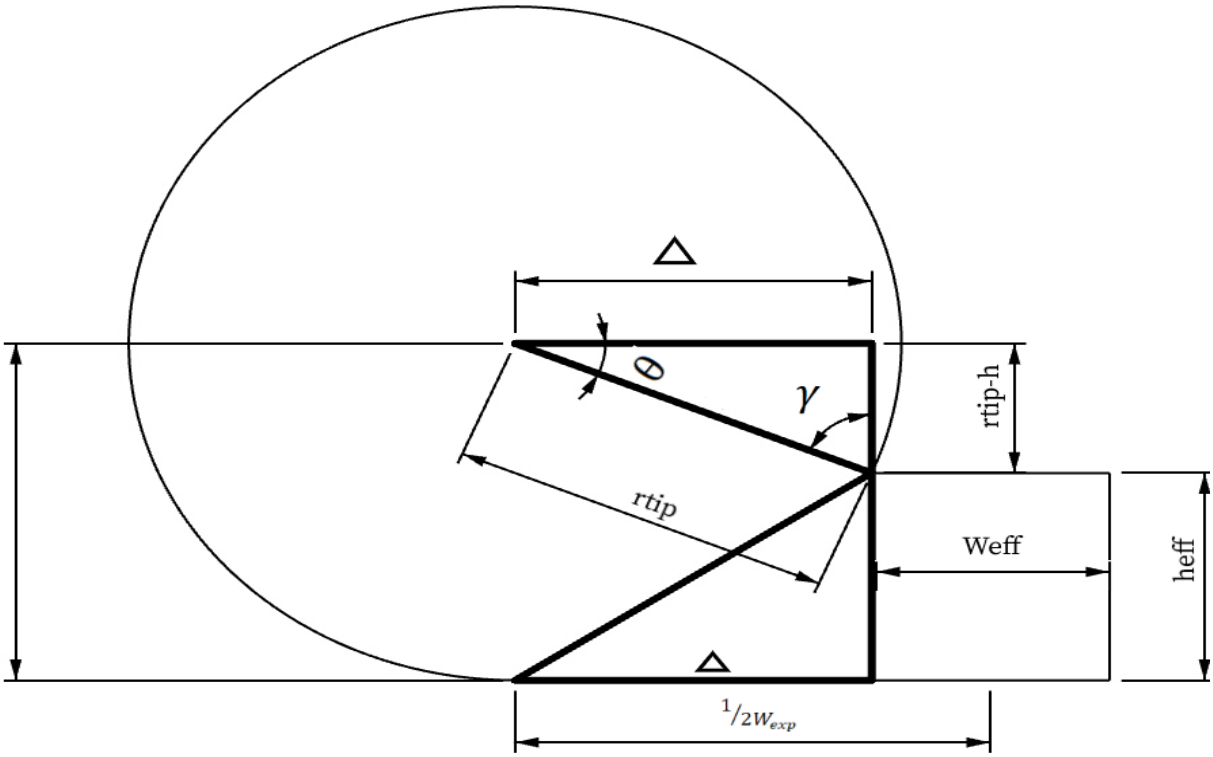

Figure 31 Schematic Diagram of case b, getting a tiny geometrical data showing actual height and imaged height

Case b	Increased size than tip round shape; circular-shaped object
Equation	$^1/_2 W_{exp} = \Delta + {}^1/_2 W_{eff}$ $\Delta = r_{tip}\, Cos \left\{ ArcSin \left[{}^{(r_{tip} - h)}/_{r_{tip}} \right] \right\}$
Height-to-tip correlation	$h = 2r_{tip}$
Position of C	C is below concerning tip round centre
Convolution	$\Delta \backsim r_{tip}$

Table 2 Geometrical calculation of convolution when a rectangular object is rectangular and Point C below the tip round centre

There can also be consideration undertaken for the rest two cases, c and d. In those cases, objects are round-shaped and more significant and smaller than tip round end, respectively. In the case c, h = r_{tip} is taken, and the convolution value is carried out. It is also noted here that point C is measured above the tip.

Case c	Increased size of an object than tip round shape, round-shaped object
Equation	$\Delta = \left(h_{eff} - r_{tip}\right) tan(\gamma)$
Height-to-tip correlation	$h = r_{tip}$
Position of C	C is above concerning tip round centre
Convolution	$\Delta = r_{tip}$

Table 3 Geometrical calculation of convolution when the circular object is rectangular and Point C above the tip round centre

Case d	Decreased size of an object than tip round shape, round-shaped object
Equation	$\Delta = r_{tip}\, Cos\left(sin^{-1}\left({\left(r_{tip} - h_{eff}\right)}/{r_{tip}}\right)\right)$
Height-to-tip correlation	$h = {}^{1}/_{2}\, r_{tip}$
Position of C	C is below concerning tip round centre
Convolution	$\Delta = 0.9\, r_{tip}$

Table 4 Geometrical calculation of convolution when the circular object is rectangular and Point C below the tip round centre

5.3.3 Object shape affecting convolution error

With these four data in hand, it can be inferred that when contact point C is located above the round tip end, convolution exhibits a distinct relationship with the tip-object angle and tip radius. In contrast, convolution does not affect the tip-object angle when contact point C is located below the round end of the tip.

Until this explanation of height dependence, the shape influence on the convolution error can also be considered. There is a deviation in effective height and width from the actual values. Such values can be co-related to the contact point C. Convolution is impacted in this situation by the object's actual height and tip radius. Aspect ratio (A = h / w) also has a significant role in convolution error. When it fluctuates and exceeds 1, the distance between L and T is more significant than predicted. When A is near

0.25, the points L and T become closer together. L=C=T for a rectangular-shaped object in its entirety. The conclusion suggests that the convolution error is less reliant on the form of items with a high A, and more on the shape of objects with low A, as discussed above.

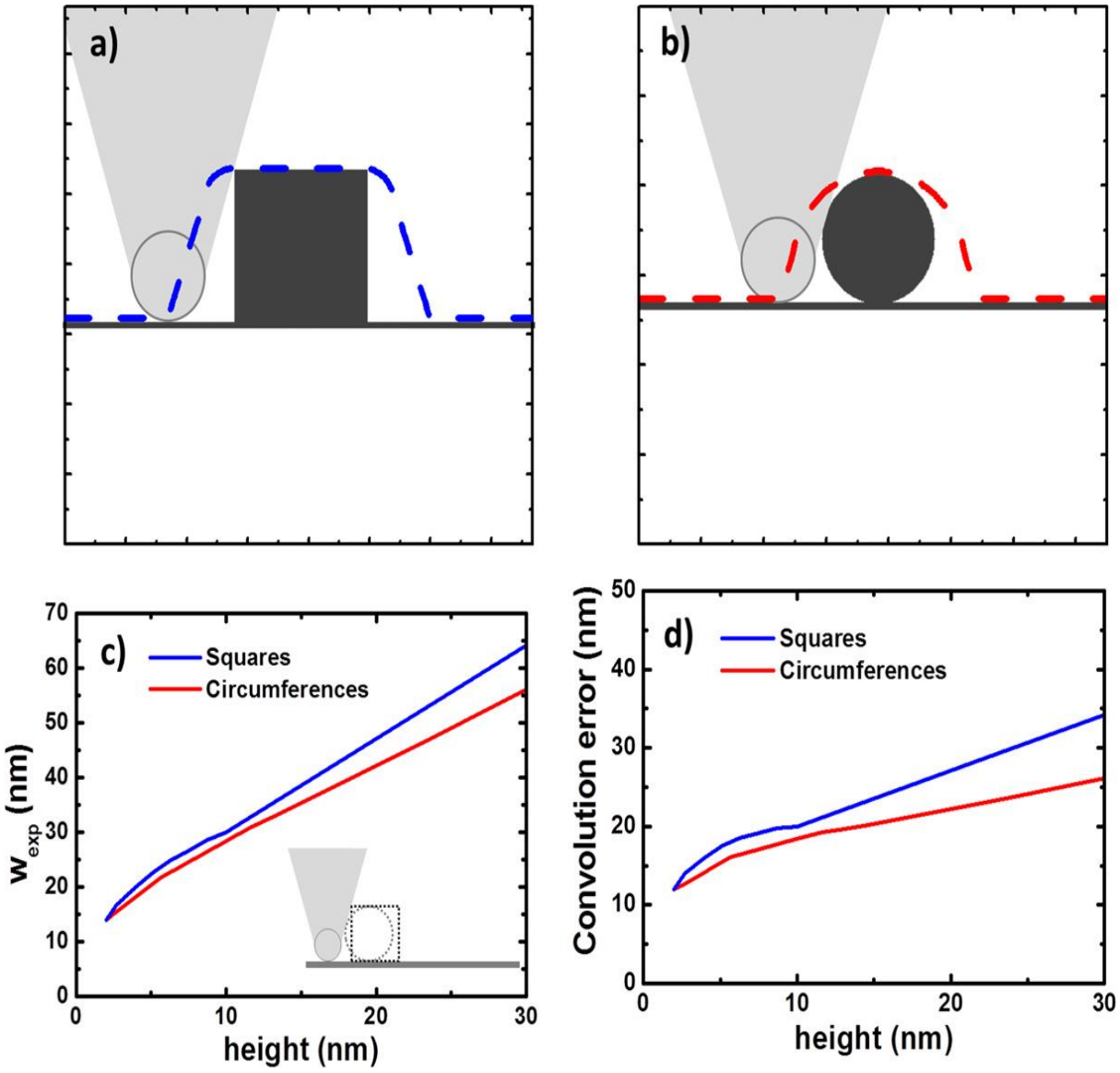

Figure 32 AFM Topography presentation using simulation series of (a) square & (b) elliptical objects at a different height. The radius of the tip has been taken 10 nm, and the tip-object angle is 19.4°. (c) and (d) shows the plots of the convolution error measured at the different height [10]

In Figure 33, the correlation between the height of the object and the convolution error is mentioned. This data has been acquired using the simulation series of the square and elliptical objects at different heights. This is also noted here that the aspect ratio is kept equal to 1 while taking the results. The tip characteristics are also used, like tip radius is 10 nm, tip- object angle is 19.4°and scale is 0.2 nm /pixel. In Figure 33 (a) and Figure 33(b), contact points can be found for both kinds of objects. Two different profile waves are created for both objects at different heights, like Blue for Squares and Red for Circular shapes. In the simulation, it is found that the contact point goes away from its origin when there is an increment in the object's height. So, the more height object has, the more away from the tip apex contact point C can be found. As the convolution error is measured ($W_{exp} - W$), for the object having height 10 nm and width 10 nm shows the effective width 35 nm having convolution error of 20 nm. This reading also proves the geometrical data of case b. As shown in Figure 33, this can be estimated that if h > r_{tip}, the contact point is above the round tip, and if not (for smaller objects than a tip round), a contact point is found into or below the round tip.

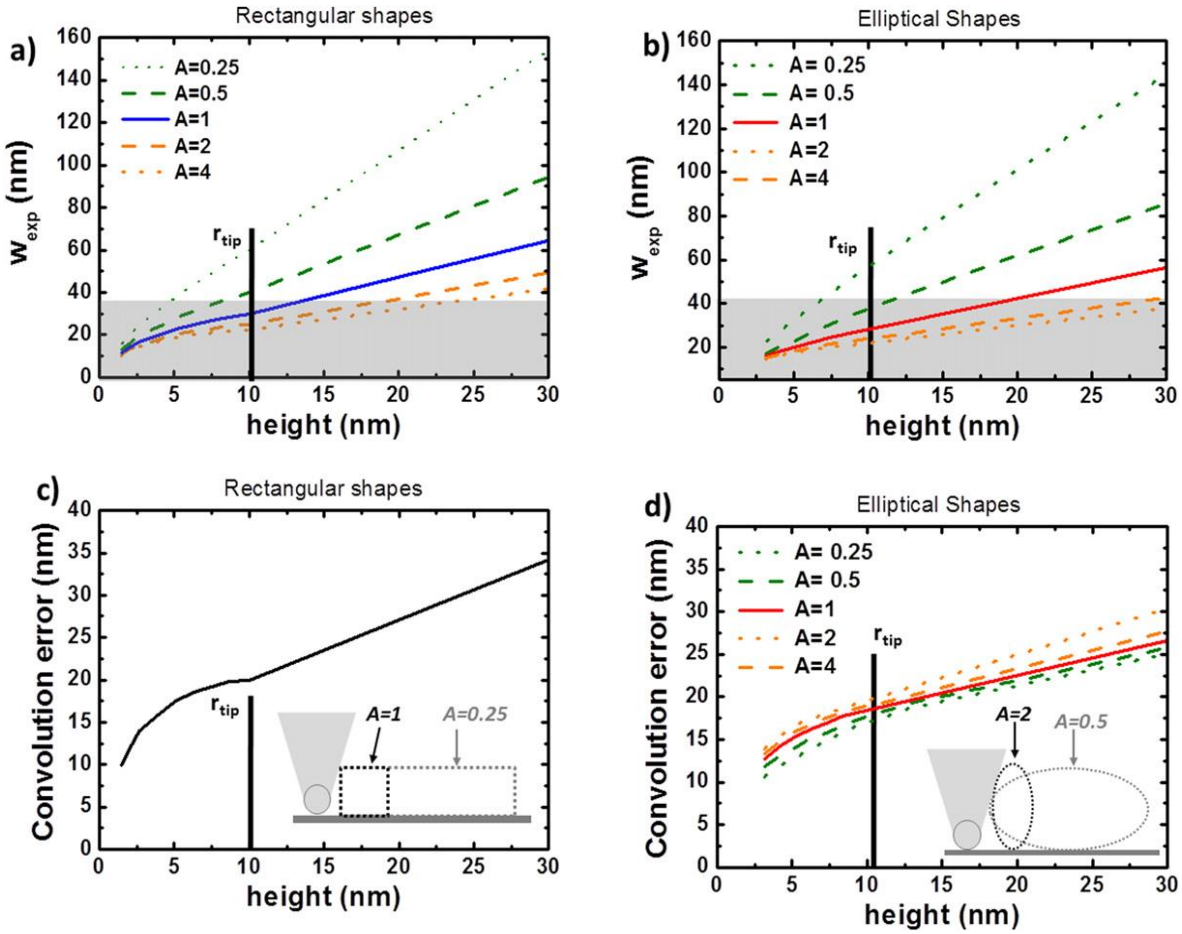

Figure 33 Results from (a) rectangular and (b) elliptical simulations displaying expected measured widths concerning their height with different aspect ratio profiles. 10 nm radius tip is set to 19.4°. In (c) and (d), convolution error is displayed regarding height with different aspect ratios. In (c), it is found that convolution generates irrespective of the aspect ratio, wherein (d) convolution error gets affected concerning aspect ratio.[10]

5.3.4 Aspect ratio affecting convolution error

As mentioned in this simulation for analysing the tendency of aspect ratio affecting the convolution error and the aspect ratio from 0.25 to 4 is observed.

Here also standard tip parameters were undertaken. Errors in elliptical forms are not entirely independent of the aspect ratio, although rectangular and elliptical shapes of the same height have comparable convolution error levels (similar convolution error values). In contrast, rectangular and round objects show a significant difference between their respective convolution error at a meagre aspect ratio of 0.25 (an object containing a height nearby 20 nm), rectangular and round objects show a significant difference between their respective convolution error. Conclusively, it can be stated that an object shape (either can be round or rectangular) has little dependence when the contact is found at the linear side region and also when the contact point below the tip round end with A < 1.

5.3.5 Tip to face angle affecting convolution error

Like other parameters, height, aspect ratio, or shape, tip angle also affects the value of convolution error. In this scenario, two different cases are observed (a) by keeping the tip to face angle constant and varying tip radius (b) by keeping the tip radius constant and varying tip to face angle. In case (a), It has been observed that below h = rt_{ip} measured profiles lead to the downward curvature and above h = r_{tip} they show a straight profile. In case (b), all profiles of different tip-face angles tend to have higher values than previous values after the height of 10 nm. In this case, there are also unique probes used lower than 10° tip-face angle. The value of convolution error increases concerning tip-face angle only if the object height is more than 10nm; however, tip-face angle does not influence the convolution error value when the object's height is less than the tip radius.

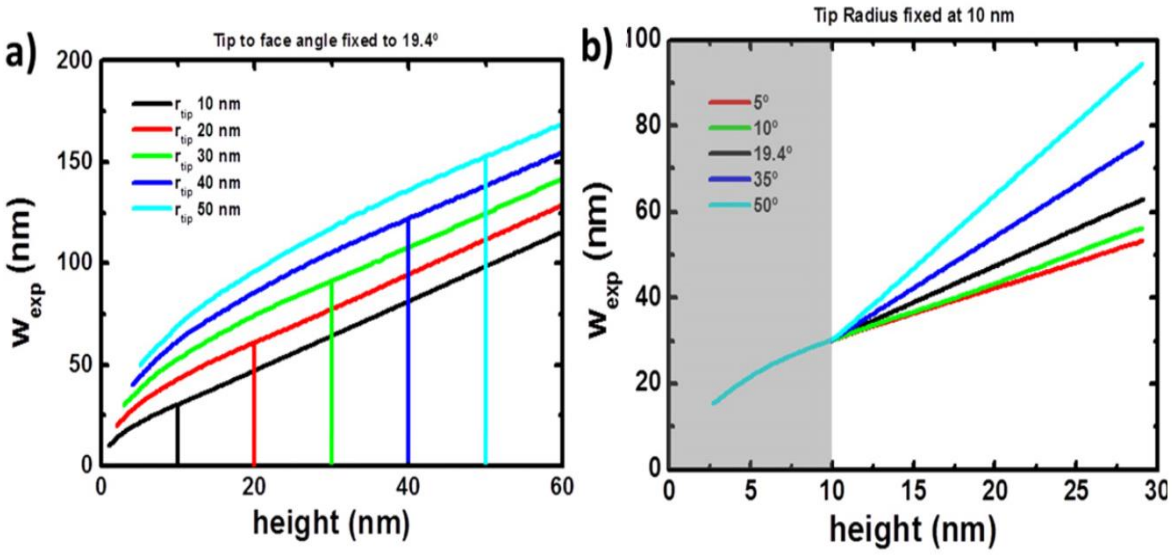

Figure 34 Tip- Face angle influence on convolution error (a) When tip- face angle was kept constant having different object height (b) When object height is constant with different tip-face angle [10]

5.3.6 Conclusion

This method of deconvolution is versatile for any tip and sample. AFM topography profiles play a significant role to simulate the rectangular and round geometries. A series simulation has been carried out to observe the dependencies of various factors like tip-face angle, object shape, aspect ratio and size. The convolution error varies mainly on a tip-face angle for an object whose height is considerable, the tip radius. However, when h decreases, the r_{tip}'s impact increases and the tip-face angle influences are negligible. Objects bigger than r_{tip} have a more substantial shape impact, whereas objects smaller than r_{tip} have convolution effects of about two r_{tip} and are mostly unaffected by shape. Because convolution errors are similar for objects as diverse as squares and circumferences in such a working range, we may conclude that the experimental error can be calculated without knowing the object form in full.

5.4 Deconvolution using software

Several other mathematical techniques have been devised and tested, as was mentioned before in this article. Image Deconvolution is a significant element of the image-processing process. Experiment artefacts like convolution effects and artefact reduction are required to improve the experiment's conclusions. The convoluted data may provide inaccurate topographic information. Modern advanced microscopy uses deconvolution as part of the process, instead of conventional imaging, which would not rely on understanding the actual surfaces or real image information.

5.4.1 Using Gwyddion Software Package

Blind tip reconstruction is a morphological algorithm that results in a deconvolution image of the AFM image. Blind tip There is no need for information about tip geometry (but tip size must be known) to deconvolve the tip shape and image convolution in this method. Software like Gwyddion has been developed using a blind tip reconstruction model. Gwyddion is a software module for visualizing and analysing SPM (scanning probe microscopy) data. This program supports several SPM data types. However, it is primarily designed to analyse height fields acquired using scanning probe microscopy methods (AFM, MFM, STM, SNOM/NSOM). It may be used for general height field and (greyscale) image processing such as profilometry or thickness maps generated by imaging spectrophotometry.

To investigate the tip's impact on the data, we must first understand the tip shape. SPM tip shape may be calculated in general in the following ways:

1. Follow the instructions provided by the manufacturer.

2. Determine the tip's characteristics using a scanning electron microscope or another independent method.

3. The use of well-established tip characterizer samples (with steep edges)

4. Using an algorithm that uses just the tip characterizers or other appropriate samples to estimate the tip

From the ways mentioned above, Gwyddion provides two of them, and it can be used either from its manufacturer data file or using an algorithm to extract the model of the tip. Gwyddion supplies two types of tips for reconstruction during the simulation of the photos. A blind tip is formed using a topography image, and a 'user customized tip' is one that the user can change the shape or size of.

After loading an AFM file, tip modelling can be performed. The second step is Data Process → SPM Modes → Tip → Model Tip. The tip size must be known before use. After getting a modelled tip, different functions can be applied. Here it must be noted that tip pixel size and physical size of the image pixel must be equal to carry out surface reconstruction. The distinction between estimated and modelled tips is that the blind estimated tip does not include additional information, unlike the model tip. The model tip is one that the user may change its design, tip-face angle, tip type, and the number of sides in the case of pyramid tips. Because blind tip reconstructions are generated using a computer algorithm, they do not include highly accurate data.

Each function has been applied and processed in the following example ZnTe (Sample image available in Gwyddion software package). The following Figure 35 depicts the topography and a three-dimensional perspective. Height and wells may be observed in 3D perspective, as well as the effect of convolution.

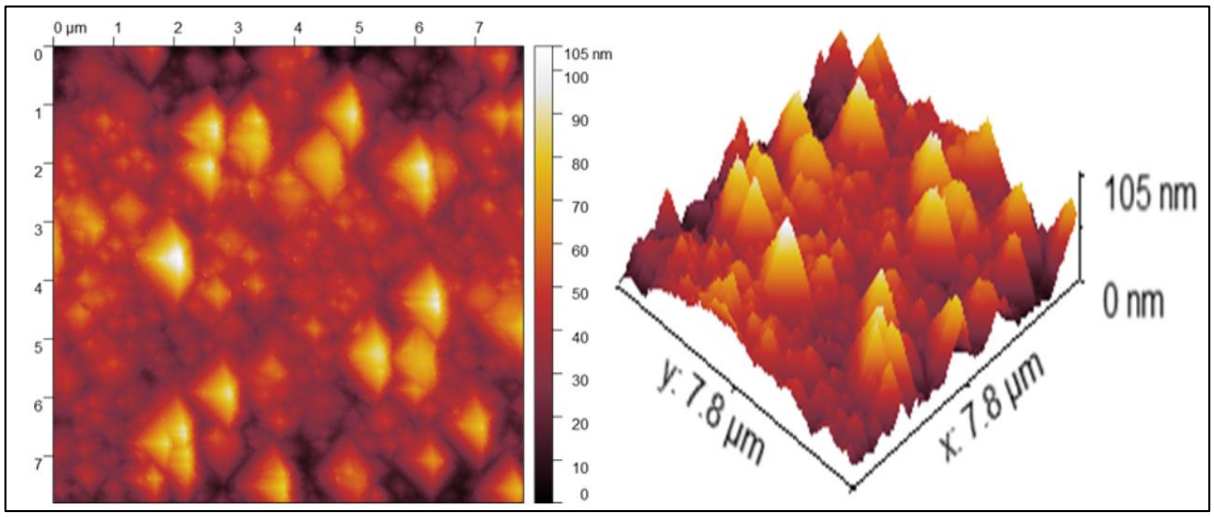

Figure 35 Left: Topography image of ZnTe surface, Right: 3D View of the same surface

The application of the reconstruction using blind tip estimate was demonstrated using an example image available from Gwyddion. This example image (in Figure 35) was captured at 500 x 500 pixels and then cropped and shrunk to 100 x 100 pixels. This clipped portion must be loaded in order to access the modelled tip in the Gwyddion toolbox. Following loading, the model tip is produced and prepared for surface reconstruction. In this case, it is essential to get a tip morphology throughout the

dilation process and a certainty map or a surface reconstruction. While re-creating an entire surface, the produced tip must be loaded first, and then the subsequent procedure applied.

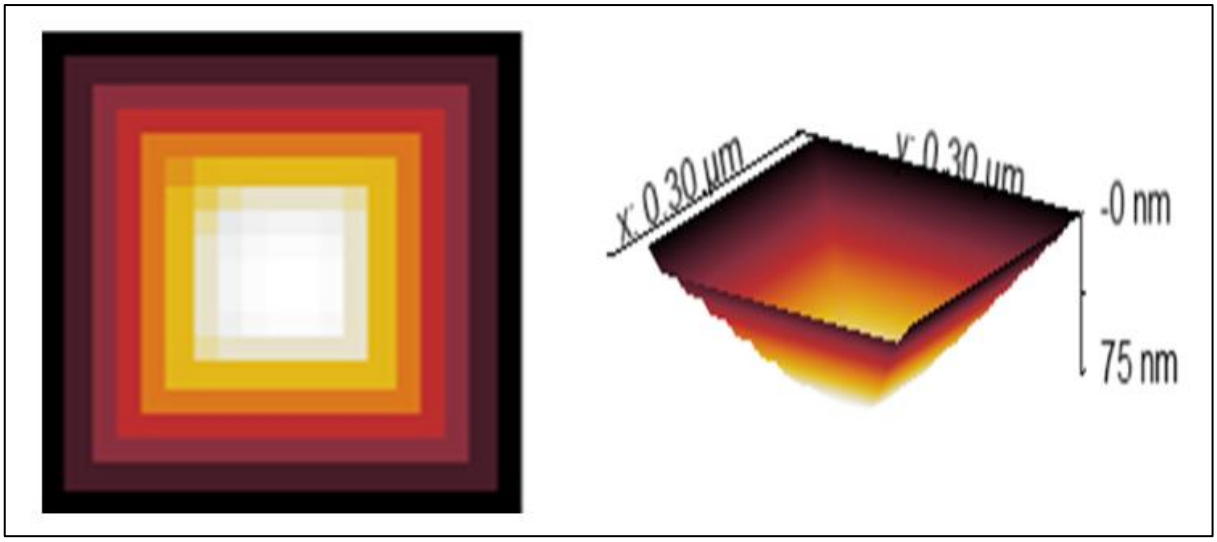

Figure 36 Left: Generated model tip using tip parameters, Right: 3D view of the same tip

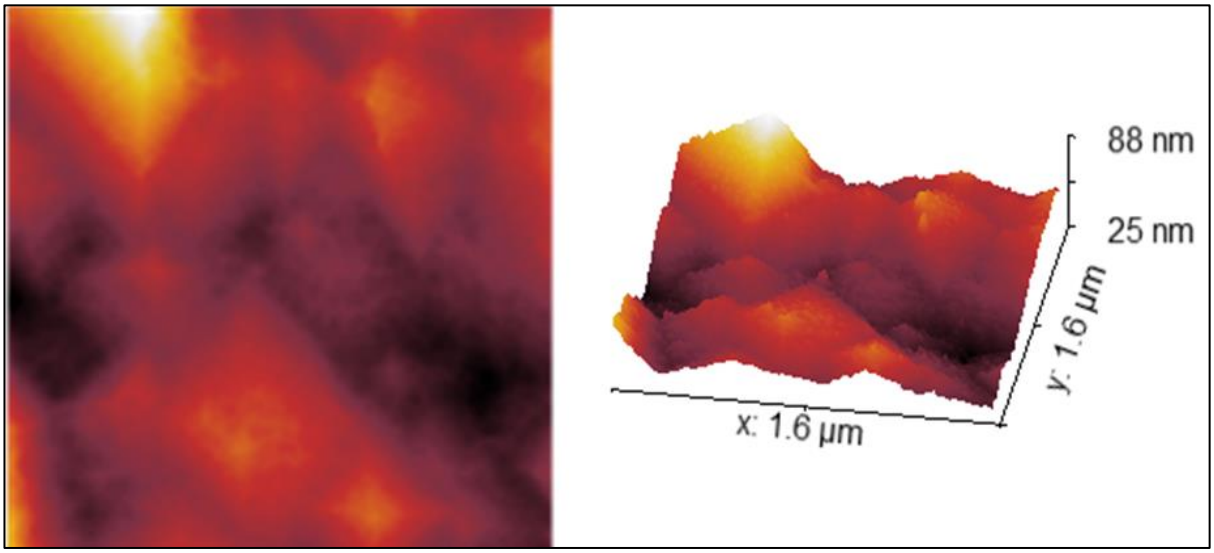

Figure 37 Left: A Part of Topography of ZnTe with equal Pixel size, Right: 3D View of the same Topography part.

As a result, in Figure 38, an accurate deconvolution cannot be performed to the actual picture surface. It would provide more accurate results with less convolution, but unlike an actual surface, such techniques would satisfy and compensate for inaccuracies to a certain degree.

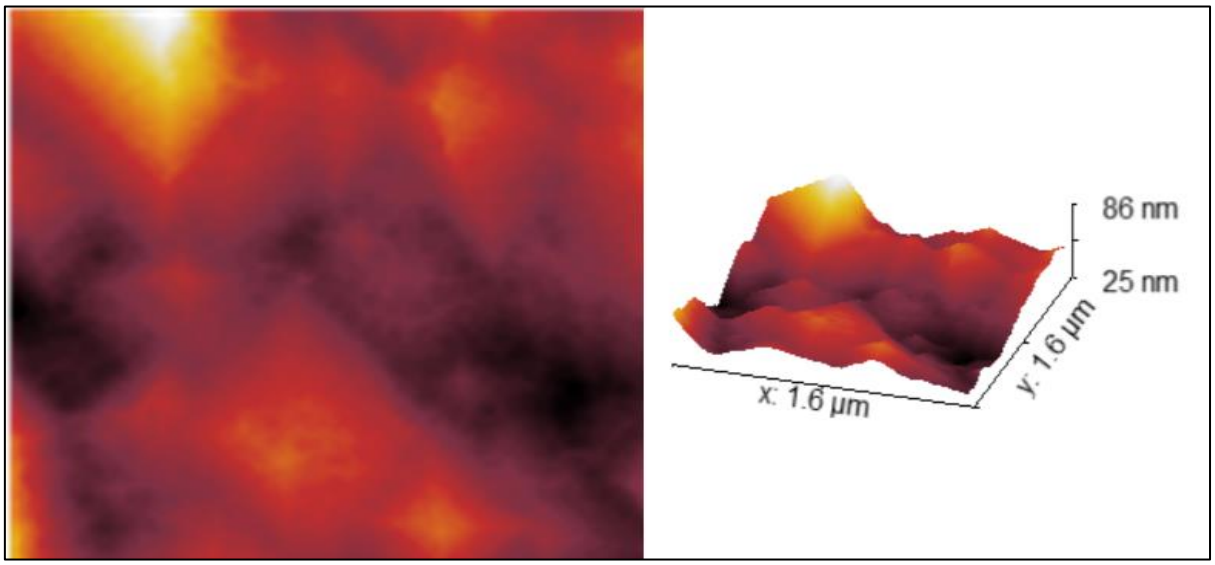

Figure 38 Left: Reconstructed surface using model tip Right: 3D View of the same reconstruction surface

5.4.2 Using SPIP Mountains 9 software

An Imaging software by Digital Surf, Mountains 9 has been developed for an entire surface and image analysis. MountainsSPIP® software provides the most sophisticated collection of professional tools for your scanning probe microscopy image analysis, based on industry-standard Mountains® technology and now incorporating all the greatest SPIPTM (Image Metrology) interaction and analytical capabilities. Various tools are available like particle analysis, examination of force curves & force volume pictures, combining SPM images with data from other instruments to do correlative analysis. Process data from ANY scanning probe microscope, including AFMs, analyse multi-channel files proper, normalize, and noise measured data ensure correct XY calibration correct tip effect Characterize surface texture in line with ISO requirements denoise, normalize, and de-noise recorded data.[20]

Additionally, regarding this project for researching image convolution and deconvolution, there are functions available for SEM pictures or any other kind of topographical data. Unlike Gwyddion software, this program has specific prerequisites, such as it must be installed on a Windows-based machine and must be operated only with the premium version. However, this program assists any AFM user in resolving

convolution and obtaining deconvolution that is as excellent as possible. The following section discusses the overview and functionality of SPIP.

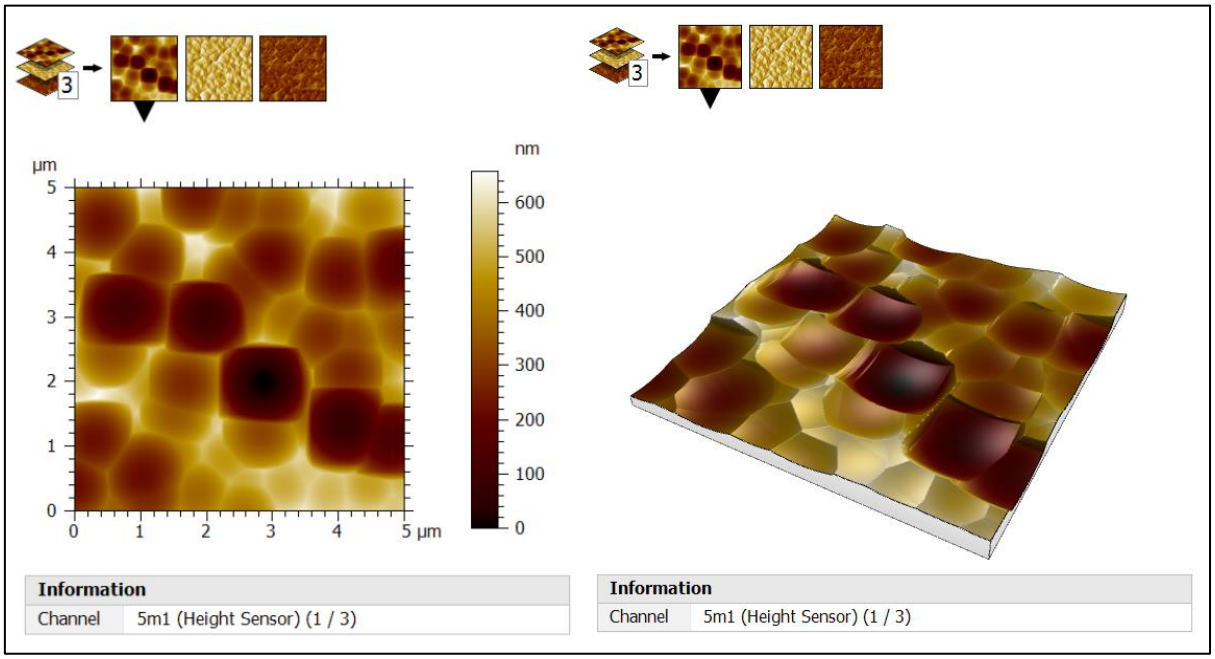

Figure 39 Left: First Channel of the topography of the Aluminia Sample, Right 3D View of the same channel

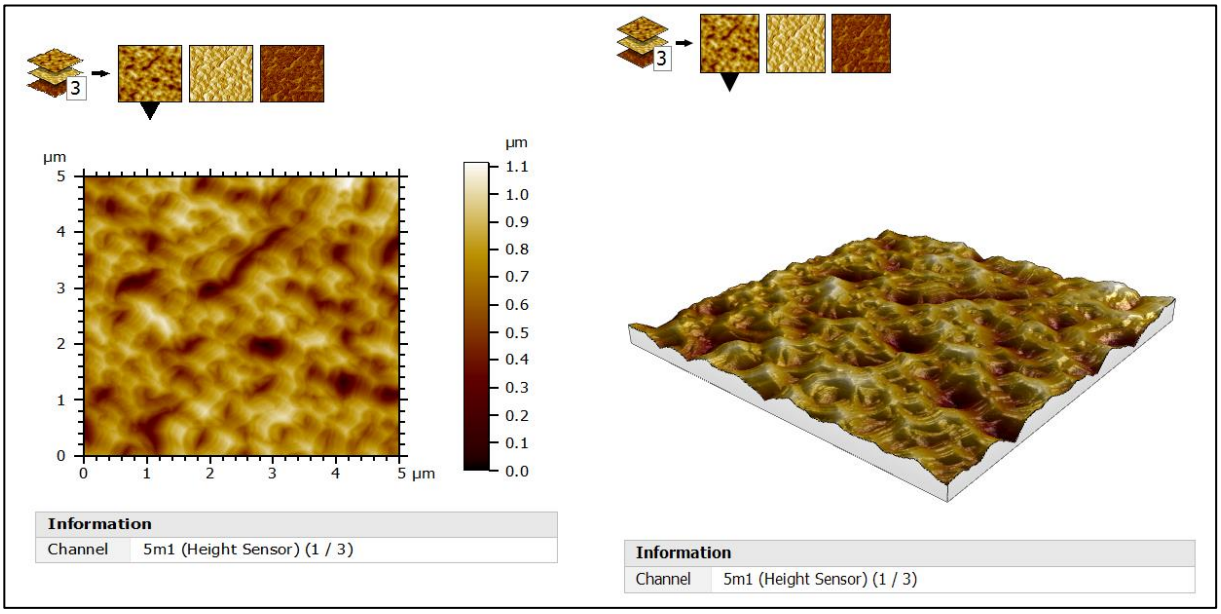

Figure 40 Left: Topography of the surface reconstruction using conispherical Modelled tip (which has the size of $(1/5)^{th}$ size of the sample), Right: 3D view of the same sample

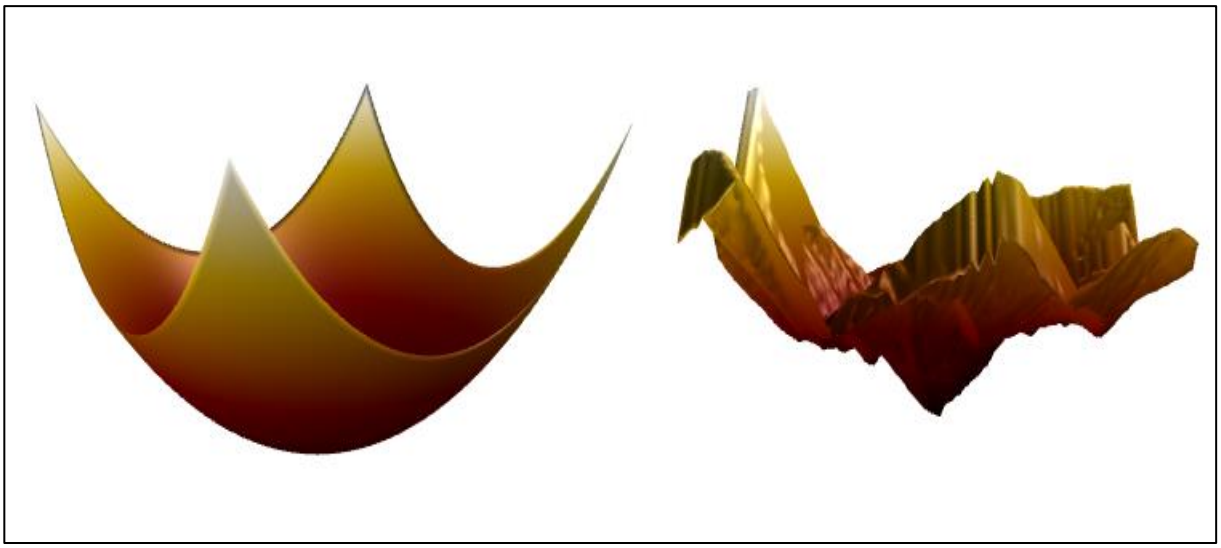

Figure 41 Left: Conispherical tip Geometry (modelled tip) created using SPIP simulation functions, Right: Tip created using Blind tip reconstruction method

In SPIP, tip deconvolution is accomplished by first imposing a desired topographic picture (in Figure 39 & Figure 40). Three channels have been analyzed for topography in this case, with the first one undergoing deconvolution. As with Gwyddion, an AFM tip must be created in SPIP in order to continue operations. AFM tip simulations may be performed either with tip reconstruction or through a standard manufactured data file.

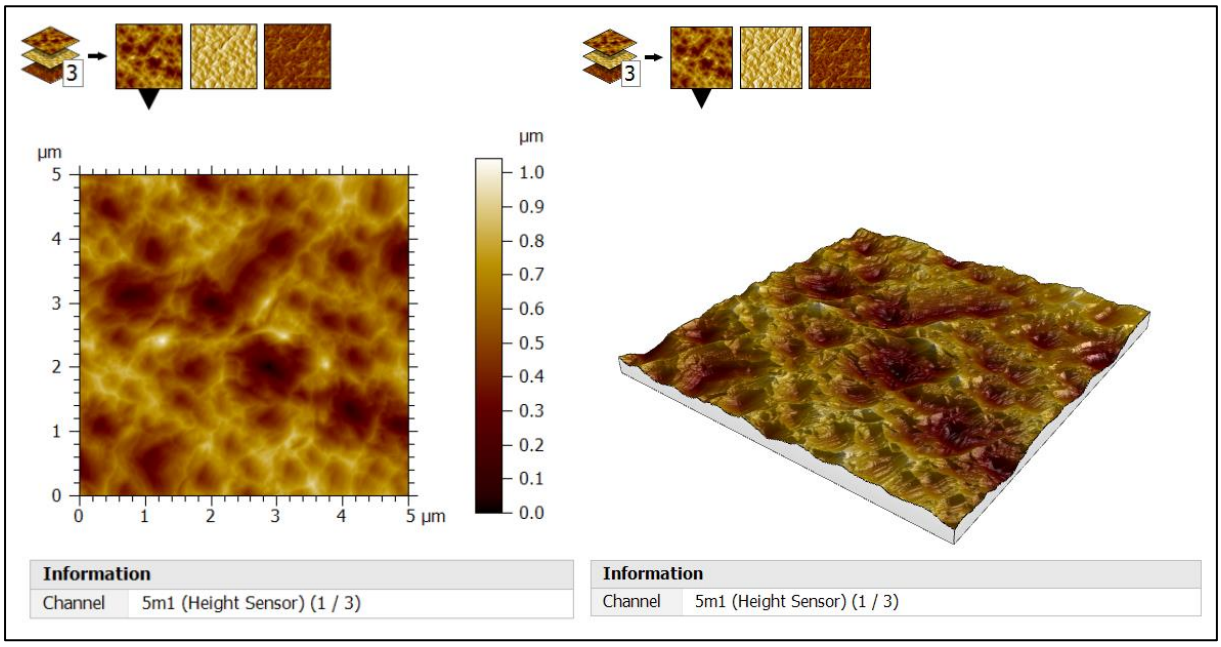

Figure 42 Left: Topography of surface reconstruction using a blind tip reconstruction, Right: 3D view of the same sample using the same tip

Although the exact information is not visible in Figure 39 (Topography), they would almost certainly have a recurring pattern of contours owing to a damaged or contaminated tip. It must be understood that such behaviour is assumed only in the absence of tip information. The tip was produced using the software's default functions in Figure 40(left). While this in-built tip generation has been implemented, other choices are available, such as simulating a parabolic tip geometry, a conical tip geometry, or both combined as conishperical. Tip size is also a consideration, such as whether it should occupy $(1/5)^{th}$ of the sample size or be optimized. Once the tip geometry has been simulated, it may be stored and reused for different samples. In Figure 41, Surface reconstruction has been applied using the modelled tip. This suggested surface reconstruction provides more comprehensive information on the roughness of the surface. Even so, this result would not be regarded as a complete, accurate deconvolution imaged as a real surface, but rather a result that is more like to an actual surface than the result of any other technique.

As stated before, blind tips may also be utilized to reconstruct surfaces. It is shown in Figure 42 (Right). In this example, a blind tip has also been used and tested to create the surface reconstruction. A customized model tip can be created by giving inputs of different parameters like height and shape. The tip is generated in the blind tip reconstruction method without asking a user for inputs. SPIP can also compute the heights and diameters of holes with any surface roughness. The chosen region in

Figure 43 has been drawn with a black and white part for heights and holes, respectively. The table below will detail the measurement data for the chosen section.

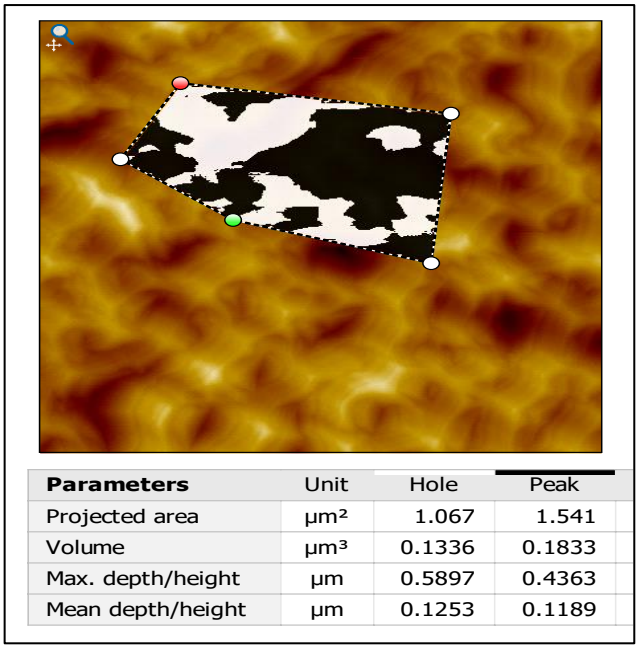

Parameters	Unit	Hole	Peak
Projected area	µm²	1.067	1.541
Volume	µm³	0.1336	0.1833
Max. depth/height	µm	0.5897	0.4363
Mean depth/height	µm	0.1253	0.1189

Figure 43 Heights and holes of selected surface area

6. Overview & Discussion

There are many techniques mentioned above in this examination of the convolution effects of the tip and subsequent deconvolution approaches. Not long ago, photo-induced force microscopy was introduced to the area of microscopy. Molecular Vista created the first PiFM setup in 2010 in the United States of America. Since then, the technique has been improved via regular upgrades. In mid-infrared PiFM, the tip shape plays an important role, as the absorption in the sample is enhanced by the simultaneous illumination of the tip [26]. This work gives an overview of image reconstruction methods available to aid the interpretation of PiFM image data. Numerous techniques for deconvolution of the imaging surface and bringing technologies closer to the actual surface of the image have been investigated over the years. However, there has not been an occurrence of a 100 per cent solution to convolution yet. However, mathematical, and geometrical techniques have been used and evaluated in this thesis so far. The following table summarizes and illustrates the approaches.

1	JOSE14 [10]	Correction of the tip convolution effects in the imaging of nanostructures studied through scanning force microscopy
2	PETE95 [13]	Atomic force microscope tip deconvolution using calibration arrays
3	BUKH97 [9]	Three-dimensional probe and surface reconstruction for atomic force microscopy using a deconvolution algorithm
4	VILL94 [23]	Morphological estimation of tip geometry for scanned probe microscopy

Table 5 Publications reviewed in this work

1	Gwyddion	Software for Surface Reconstruction, Blind tip construction
2	SPIP	Sofware for Image analysis, Topography analysis, Tip Deconvolution, Surface reconstruction

Table 6 Software studied in this work

To begin, analysing the summary of JOSE14, which examined convolution and deconvolution of AFM images. Different shapes and tip geometries may interact, and this idea can be accomplished. Specifically, only elliptical and rectangular objects have been examined and analysed in Canet's and his colleagues' explanations. The mathematical model for deconvolution is not very complicated; instead, it includes fundamentals of geometry that contributed to the solution of deconvolution. The same team also created MATLAB deconvolution. However, its matrices must be generated

using particular examples. Additional explanation about the simulation of matrices, the AFM tip, the sample to be tested, and the canvas containing the tip and sample must be created with appropriate resolutions. For example, tip (513 x 513), sample (1026 x 513), and canvas (1026 x 1026) pixels must be created from their SEM photographs. This simulation may be processed by adding a tip matrix and a sample matrix to the whole canvas. Convolution may be eliminated by observing the tip's movement toward the target. This technique does have certain drawbacks, such as the requirement to estimate a matrix for each SEM picture. However, since no tip information is assumed in the whole calculation, this simplification and original technique of JOSE14 shows itself to be a severely impacted method. The manufacturer's user manual or SEM were used to obtain all of the AFM Tip's comprehensive information. JOSE14 would also address convolution effects and seek an actual optimized surface; however, the geometry of the objects and tips should be as specified. As stated in 5.2, objects as rectangular and elliptical as feasible may compensate for the inaccuracies and solution provided by JOSE14. Despite creating a concept for producing a similar technique for many other forms, a different shape of the item and AFM tip would not meet the input criteria of this method.

PETE95 is also an efficient deconvolution technique since it has a new kind of context. Rather than a mathematical computation, it includes a mask preparation procedure. Convolution of the tip may be resolved by creating a surface mask on a limited portion of the surface roughness. It should be emphasized that this technique does not primarily involve the reconstruction of the surface but rather the development of a mask for a tip. Due to the critical significance of tip geometry in deconvolution, this suggested explanation cannot be contradicted.

In contrast to JOSE14, PETE95 recommends tip convolution, whereas JOSE14 focuses only on surface convolution error levels. Even though PETE95's approach does not include a reconstruction step, it may be approximated from convolution error numbers. JOSE14 has the disadvantage of requiring each contour to be simulated and covered to get a tip geometry. It cannot be claimed that a single contour, height, or hole can provide a suitable tip geometry; a series of simulations for various parts of the surface must be performed. As explained, application of this method for rectangular shape objects differs for round shapes. Simulation to get convolution error value would consume more time than only having a reconstruction surface.

In addition to these two ways, BUKH97 has also established the existence of an initial idea for reconstructing surfaces. Instead of producing a tip geometry, this method emphasizes the Inverted tip. This method has a disadvantage when the tip gets convoluted because it only considers reconstruction when calculating the overall process. If users move an inverted tip over a surface contour while it is contaminated or double-tipped, they will get the same results. As a result, surface convolution effects can be corrected, but tip convolution will remain unchanged using this strategy. This scenario is true more or less for every method, but it needs to be emphasized here because BUKH97 mainly works with the tip. BUKH97, like JOSE14, demands applying

the technique to the entire surface rather than just a portion of it. BUKH97 works only with the inverted tip movement on the surface irrespective of tip geometry, while JOSE14 itself depends on the creation of tip geometry. As previously stated, optimizing tip geometry can be achieved by running a series of simulations on different surface areas (not the entire surface). However, in BUKH97, every pixel on the surface must be processed to obtain a surface reconstruction.

The deconvolution using reconstruction methods or by making a tip geometry claims various aspects (Blind tip construction, user Customized tip, inverting tips, different object contour shapes) of their application because one or another way every method provides deconvolution to some extent. Every method claims a deconvolution procedure irrespective of advantages and disadvantages. So far, suggested methods rely on the tip geometry or creating a tip geometry. Method conception using VILL94 suggests Blind tip construction. In Blind tip construction, information of AFM tip is not needed. This method was just created using the morphological methodology, and further using it, various software has been designed. Software like Gwyddion and SSIP also prove blind tip construction. This software work more or less for surface reconstruction than only just the creation of tip geometry. In general, SSIP would give more functionality than just a reconstruction. Gwyddion was created long ago and upgraded regularly. Gwydidion interface does not contain very modern tools to analyse images and surfaces, and it gives some essential image analysis tools. SSIP focuses more on tip deconvolution and reconstruction, including having various tools and functions to apply over it. The main drawback found for SSIP is that it has to be a premium version for regular use, while Gwyddion is open source for any user.

Conclusively, various methodologies have been created to improve the field of surface engineering in all directions. Microscopy technology has advanced and is still being improved even today, from merely obtaining an image's topography to obtaining every piece of surface information. Instead of merely topographical imaging with SEM, atomic force microscopy is critical for obtaining thorough information about any sample structure. Every other AFM user expects the measured picture to be deconvoluted because of the numerous convolution effects in AFM. To obtain the best deconvolution, researchers looked at a variety of approaches. In order to generate tip geometry or directly reconstruct the surface, each approach has its unique input requirements. One can also get help from various available software to remove artefacts. Having detailed information on an AFM tip could also help a user get rid of errors.

Suggested methods can be applied to PiFM data. A series of simulation experiments could be executed for further deconvolution analysis, and convolution artefacts can be avoided. PiFM data of known and regular surfaces are required to do such analysis. As discussed so far, there are different ways to compensate artefacts for different samples. Knowing artefacts of regular experiments and being familiar with samples would raise chances to apply deconvolution methods more accurately.

7. Bibliography

[1] *Nila Krishnakumar (2019): PHOTO INDUCED FORCE MICROSCOPIC AND SPECTROSCOPIC (IR AND RAMAN) CHARACTERISATION OF NANOMATERIALS. Master Thesis, Jena, Germany. Leibniz Institute of Photonics Technologies.*

[2] *Eaton, Peter; West, Paul (2010): Atomic Force Microscopy: Oxford University Press.*

[3] *Dr R. Mukherjee (2013): Atomic Force Microscopy. Instability and Patterning of Thin Polymer Films. Kharagpur, India: Department of Chemical Engineering, IIT Kharagpur. Available online at https://nptel.ac.in/courses/103/105/103105066/, checked on 4/24/2021.*

[4] *Molecular Vista: Photo-induced Force Microscopy Scientific Principles. Available online at https://molecularvista.com/technology/photo-induced-force-microscopy-and-spectroscopy/, checked on 4/13/2021.*

[5] *Braga, Pier Carlo; Ricci, Davide (2004): Atomic Force Microscopy: Biomedical Methods and Applications. Methods in Molecular Biology. 242 volumes. Totowa, NJ: Humana Press (Methods in Molecular Biology™, 242).*

[6] *Murdick, Ryan A.; Morrison, William; Nowak, Derek; Albrecht, Thomas R.; Jahng, Junghoon; Park, Sung (2017): Photo-induced force microscopy: A technique for hyperspectral nanochemical mapping. In Jpn. J. Appl. Phys. 56 (8S1), 08LA04. DOI: 10.7567/JJAP.56.08LA04.*

[7] *Nanoscience Instruments (2019): Atomic Force Microscopy - Nanoscience Instruments. Available online at https://www.nanoscience.com/techniques/atomic-force-microscopy/, updated on 1/25/2019, checked on 4/19/2021.*

[8] *N. Krishnakumar, A. Strecker, M. Luo, R. Lachmann, R. Heintzmann, P. Biehl, F.H. Schacher, U. Neugebauer, D. Täuber, Insights from application of photo-induced force microscopy (PiFM) for investigation of multicore magnetic nanoparticles (MCNPs). 2020 NanoScientific Forum Europe, September 2020.*

[9] *Bukharaev, A.; Berdunov, Nikolai; Ovchinnikov, D.; Salikhov, K. (1998): Three-dimensional probe and surface reconstruction for atomic force microscopy using deconvolution algorithm. In Scanning Microsc 12.*

[10] *Canet-Ferrer, Josep; Coronado, Eugenio; Forment-Aliaga, Alicia; Pinilla, Elena (2014): Correction of the tip convolution effects in the imaging of nanostructures studied through scanning force microscopy. In Nanotechnology 25, p. 395703. DOI: 10.1088/0957-4484/25/39/395703.*

[11] *Daniela Täuber (2020): POLIRIM: "Continuation of fundamental investigations with polarization-resolved IR spectroscopy and photo-induced atomic force microscopy (PiFM) for biomedical application".*

[12] *Laia Canet-Ferrer, Josep; Coronado, Eugenio; Forment-Aliaga, Alicia; Pinilla, Elena (2014): Supporting Information of Correction of the tip convolution effects in the imaging of nanostructures studied through scanning force microscopy.*

[13] *Markiewicz, Peter; Goh, M. Cynthia (1995): Atomic force microscope tip deconvolution using calibration arrays. In Review of Scientific Instruments 66 (5), pp. 3186–3190. DOI: 10.1063/1.1145549.*

[14] *Marques-Moros, Francisco; Forment-Aliaga, Alicia; Pinilla, Elena; Canet-Ferrer, Josep (2020): Mirror effect in atomic force microscopy profiles enables tip reconstruction. In Scientific Reports 10. DOI: 10.1038/s41598-020-75785-0.*

[15] *Molecular Vista (2021): Principles - Photo-induced force microscopy and spectroscopy. Available online at https://molecularvista.com/technology/PiFM-and-pif-ir/scientific-principles/, updated on 10/11/2021, checked on 10/12/2021.*

[16] *Molecular Vista (2021): Featuring Vista Series microscopes. Available online at molecularvista.com, checked on 10/12/2021.*

[17] *Petr Klapetek; David Nečas; and Christopher Anderson: Gwyddion user guide. Available online at http://gwyddion.net/download/user-guide/gwyddion-user-guide-en.pdf, checked on 12/10/2021.*

[18] *Richard Miller; James Vesenka; Eric Henderson (1995): Tip Reconstruction for the Atomic Force Microscope. In SIAM Journal on Applied Mathematics 55 (5), pp. 1362–1371. Available online at http://www.jstor.org/stable/2102579.*

[19] *Robin Schneider (2021): Application of IR-based nanospectroscopic methods to study the interaction of Vancomycin with the bacterial cell wall of Bacillus subtilis. Master Thesis, Jena, Germany. Leibniz Institute of Photonic Technology.*

[20] *Surface Metrology Guide - Digital Surf (2021). Available online at https://guide.digitalsurf.com/en/guide.html, updated on 3/19/2021, checked on 10/12/2021.*

[21] *Tabet, M. F. (1997): Deconvolution of tip affected atomic force microscope images and comparison to Rutherford backscattering spectrometry. In J. Vac. Sci. Technol. B 15 (4), p. 800. DOI: 10.1116/1.589412.*

[22] *Udpa, L.; Ayres, V. M.; Fan, Yuan; Chen, Qian; Kumar, S. A. (2006): Deconvolution of atomic force microscopy data for cellular and molecular imaging. In IEEE Signal Process. Mag. 23 (3), pp. 73–83. DOI: 10.1109/MSP.2006.1628880.*

[23] *Villarrubia, J. S. (1994): Morphological estimation of tip geometry for scanned probe microscopy. In Surface Science 321 (3), pp. 287–300. DOI: 10.1016/0039-6028(94)90194-5.*

[24] *Villarrubia, J. S. (1997): Algorithms for Scanned Probe Microscope Image Simulation, Surface Reconstruction, and Tip Estimation. In J. Res. Natl. Inst. Stand. Technol. 102 (4), pp. 425–454. DOI: 10.6028/jres.102.030.*

[25] *Jahng, J. (2015). Photo-induced force microscopy and spectroscopy.* UC Irvine*. ProQuest ID: Jahng_uci_0030M_13272. Merritt ID: ark:/13030/m5xp9c5v. Retrieved from https://escholarship.org/uc/item/84g776h2*

[26] *Jahng, J.; Potma, E. O.; Lee, E. S. Nanoscale Spectroscopic Origins of Photoinduced Tip-Sample Force in the Midinfrared. Proc. Natl. Acad. Sci. U. S. A. 2019, 116 (52), 26359–26366*

[27] *Hardikkumar Gadher, Master Thesis Project Proposal, TIP CONVOLUTION EFFECTS AND ITS DECONVOLUTION IN PHOTO INDUCED FORCE MICROSCOPY, 2021*

[28] *Franze, K., Gerdelmann, J., Weick, M., Betz, T., Pawlizak, S., Lakadamyali, M, Käs, J. (2009). Neurite branch retraction is caused by a threshold-dependent mechanical impact. Biophysical Journal, 97(7), 1883–1890. https://doi.org/10.1016/j.bpj.2009.07.033*

[29] *N. Krishnakumar, A. Strecker, M. Luo, R. Lachmann, R. Heintzmann, P. Biehl, F.H. Schacher, U. Neugebauer, D. Täuber, Insights from the application of photo-induced force microscopy (PiFM) for investigation of multicore magnetic nanoparticles (MCNPs). 2020 NanoScientific Forum Europe, September 2020.*